Institute of Thermoelectricity, Academy of Sciences and Ministry of Education and Science of Ukraine

# Journal of THERMOELECTRICITY

International Research

Founded in December, 1993

published 6 times a year

*No. 5* *2015*

## Editorial Board



## International Editorial Board

Founders – National Academy of Sciences, Ukraine
Institute of Thermoelectricity of National Academy of Sciences and Ministry of Education and Science of Ukraine

Certificate of state registration № КВ 15496-4068 ПР

Editorial office manager O. Pugantseva



Approved for printing by the Academic Council of Institute of Thermoelectricity of the National Academy of Sciences and Ministry of Education and Science, Ukraine

Address of editorial office:
Ukraine, 58002, Chernivtsi, General Post Office, P.O. Box 86.
Phone: +(380-372) 90 31 65.
Fax: +(380-3722) 4 19 17.
E-mail: jt@inst.cv.ua
http://www.jt.inst.cv.ua

Signed for publication 25.11.15. Format 70×108/16. Offset paper №1. Offset printing.
Printer's sheet 11.5. Publisher's signature 9.2. Circulation 400 copies. Order 5.

Printed from the layout original made by "Journal of Thermoelectricity" editorial board in the printing house of "Bukrek" publishers,
10, Radischev Str., Chernivtsi, 58000, Ukraine

**CONTENTS**

**L.I. Anatychuk[1,2], L.N. Vikhor[1], P.V. Gorskiy[1]**

[1]Institute of Thermoelectricity of the NAS and MES of Ukraine,
1, Nauky Str., Chernivtsi, 58029, Ukraine;
[2]Yu.Fedkovych Chernivtsi National University
Chernivtsi, Ukraine, 58012, 2, Kotsyubinsky str.

# OPTIMIZATION OF *Bi-Te* BASED MATERIALS FOR THERMOELECTRIC ENERGY CONVERTERS UNDER THE CONDITIONS OF MINIATURIZATION

*Based on the temperature and concentration dependences of the kinetic coefficients of thermoelectric material (TEM), the concentration dependences of thermoelectric figure of merit of TEM were determined under the conditions of miniaturization for thermoelectric cooling and generation modes with different layer thicknesses. In so doing, the microscopic parameters of TEM necessary for taking into account the impact of size effects were directly determined on the basis of approximation models of their kinetic coefficients. The impact of size effects on the electrical conductivity of TEM was taken into account in the approximation of constant with respect to energy mean free path of charge carriers, and their impact on the lattice thermal conductivity – with regard to frequency dependence of the relaxation time of phonons scattered on each other due to anharmonicity of lattice thermal vibrations. In the latter case, both Umklapp and normal processes were considered capable of modifying scattering of electrons at layer boundaries. It was shown that with reduction of TEM layer thickness to 50 μm a gain in the figure of merit as compared to single crystal is 1 – 4 %. For lower thicknesses a gain can be greater. In particular, with reduction of TEM layer thickness to 0.1 μm, maximum thermoelectric figure of merit is increased by a factor of 1.7 – 3.2 against single crystal. In so doing, reduction of TEM layer thickness to 50 μm scarcely affects the optimal concentration of doping single-charge impurities, whereas transition to lower thicknesses reduces it. For instance, with the layer thickness 0.1 μm it is reduced by a factor of 1.1 – 2.2 as compared to single crystal.*

**Key words:** electric conductivity, thermoEMF, thermal conductivity, phonons, charge carriers, relaxation time, normal processes, Umklapp processes, mean free path, thermoelectric figure of merit.

## Introduction

Miniaturization of thermoelectric energy converters is a relevant task of up-to-date functional electronics. The need for miniaturization is primarily dictated by considerations of reduced consumption of thermoelectric material which is the most expensive part of these converters. Moreover, earlier studies pursued by various authors on the powders, films and wires of thermoelectric materials [1 – 5] give certain grounds to believe that miniaturization will not degrade the output characteristics of thermoelectric energy converters, and even will improve them as compared to characteristics of converters based on the bulk single crystals.

It is common knowledge that the figure of merit of TEM depends on the concentration of charge carriers, hence, of doping impurities [6]. Moreover, for each temperature there exists such optimal charge carrier concentration whereby the figure of merit is maximal. However, when passing from single crystals to thin layers, the effects related to charge carrier and phonon scattering at layer boundaries become apparent. In so doing, the kinetic coefficients of TEM are changed, hence, the maximum figure of merit and the corresponding optimal concentration of charge carriers can vary. Therefore, the purpose of this paper is optimization of TEM for charge carrier concentration under the conditions of the impact of TEM layer thickness on its kinetic coefficients.

## Method of estimation of the figure of merit of TEM thin layers versus their thickness and charge carrier concentration

Taking into consideration that layer boundary scattering has no impact on thermoEMF, and electron thermal conductivity and electrical conductivity in case of energy independence of electron mean free path depend on layer thickness through the same multiplier [7, 8], one can readily derive the following expression for the figure of merit $Z$ of thin layer with respect to single crystal $Z_{mono}$:

$$Z/Z_{mono} = \frac{1+\kappa_{n,p(mono)}/\kappa_{l(mono)}}{Z_a^{-1}+\kappa_{n,p(mono)}/\kappa_{l(mono)}}. \tag{1}$$

In this formula

$$Z_a = \left\{d_0 l_{n,p}^{-1}\ln\left[1+l_{n,p}d_0^{-1}\right]\right\}^{-1}\left[\int_0^1\int_0^1 \frac{x^4\exp(x/\theta)}{\left[\exp(x/\theta)-1\right]^2}\left(\frac{k_{||}^* z}{1+k_{||}^* Q_{l||}(x)z}+\frac{2k_{||}^* z}{1+k_{||}^* Q_{t||}(x)z}\right)dzdx\right]^{-1}\left\{\int_0^1 \frac{x^4\exp(x/\theta)}{\left[\exp(x/\theta)-1\right]^2}\left(\frac{1}{Q_{l||}(x)}+\frac{2}{Q_{t||}(x)}\right)dx\right\}. \tag{2}$$

In formulae (1 – 2), the following notations are introduced: $\kappa_{n,p(mono)}$ – electron or hole components of full thermal conductivity of single crystal, $\kappa_{l(mono)}$ – its lattice component, $d_0$ – layer thickness, $l_{n,p}$ – mean free path of electrons (holes) in single crystal, $k_{||}^* = \left(d_0\gamma^2\theta/\rho\right)\left(k_B T_D/\hbar v_{||}\right)^4\left(k_B T_D/\rho v_{||}^2\right)$, $\theta = T/T_D$, $T$ – absolute temperature, $T_D$ – the Debye temperature of material, $\gamma$, $\rho$ and $v_{||}$ – the Gruneisen parameter, the density and velocity of sound in TEM, respectively, $k_B$ – the Boltzmann constant, the rest of notations are commonly accepted. Index "||" means that the corresponding parameter is taken in a direction parallel to layer plane of TEM. Frequency polynomials $Q_{l||}(x)$ and $Q_{t||}(x)$, accordingly, are given below:

$$Q_{l||}(x) = x^4 + \mu x, \tag{3}$$

$$Q_{t||}(x) = \left(\mu + 3.125\,\theta^3\right)x. \tag{4}$$

Formulae (3) and (4) take into account both normal and Umklapp processes for the longitudinal (*l*) and transverse (*t*) phonon modes. Component $\mu x$ is responsible for Umklapp processes. It is also taken into account that phonon scattering due to normal processes takes place differently for the longitudinal and transverse modes, which is adequately described by other components in (3) and (4).

Relation (2) with regard to (3) and (4) was derived with the use of approaches developed in [7, 8] for the cases of spherical particles and contacts between them, however, these approaches were modified with regard to specific geometry of charge carriers and phonons in a thin TEM layer.

Thus, from relations (1 – 4) we see that for the calculation of thermoelectric figure of merit and efficiency of thin layers one must, using the experimental data, preliminarily divide full thermal conductivity of single crystal into a component caused by electrons (holes) and lattice thermal conductivity. Also, based on the experimental data of the dependences of electrical conductivity, thermoEMF and thermal conductivity of single crystal on the temperature and charge carrier concentration, it is necessary to determine the temperature and concentration dependences of mean free path of electrons (holes) $l_{n,p}$ and parameter $\mu$ which is responsible for phonon scattering and, hence, for the value of TEM lattice thermal conductivity.

## Determination of the microscopic parameters of TEM based on the approximation of their kinetic coefficients

To determine the above microscopic parameters, the approximation models of experimental dependences of the kinetic coefficients of TEM are used that are built, for instance, by least-squares method [9]. On the basis of these models the microscopic parameters of TEM are determined as follows.

At first, on the assumption of energy independence of the mean free path of charge carriers, by the concentration and temperature-dependent thermoEMF from Eq. [10]

$$\alpha = \frac{k_B}{e}\left[\frac{2F_1(\eta)}{F_0(\eta)} - \eta\right] \tag{5}$$

the reduced chemical potential $\eta = \zeta / k_B T$ is determined. Following that, on the assumption of impurity conductivity, from the equation of constancy of the number of particles [10]

$$n_0 = \frac{4\left(2\pi m^*_{n,p} k_B T\right)^{3/2}}{\sqrt{\pi} h^3} F_{1/2}(\eta) \tag{6}$$

by the known density-of-state mass of electrons (holes) $m^*_{n,p}$, for instance, at temperature 300 K, charge carrier concentration $n_0$ is determined. Then, at each fixed concentration $n_0$ the temperature dependence of density-of-state effective mass $m^*_{n,p}$ is found. There is another method

which is realized with the availability of data on charge carrier mobility. At first, charge carrier concentration is determined by the conductivity and mobility, and then from Eq. (6) – the density-of-state effective mass.

Following that, by the experimental temperature and concentration dependences of the electrical conductivity the mean free path of electrons (holes) $l_{n,p}$ on the temperature and charge carrier concentration is determined. For this purpose we employ the relation for the case of energy-independent mean free path of electrons (holes) [4]:

$$\sigma_{mono} = \frac{4n_0 e^2 l_{n,p} F_0(\eta)}{\sqrt{2m^*_{e,h} k_B T} F_{1/2}(\eta)}. \tag{7}$$

In formulae (5) – (7), $F_r(\eta)$ – the Fermi integrals of corresponding indices determined by the relation:

$$F_r(\eta) = \int_0^\infty \frac{x^r dx}{\exp(x-\eta)+1}. \tag{8}$$

Concerning the use of relation (6) for the determination of carrier concentration it should be noted that density-of-state effective mass of electrons (holes) is a function of not only temperature, but also charge carrier concentration. However, in case of materials for coolers an argument of approximation models is not charge carrier concentration, but the electric conductivity at 300 K. For this case a simplifying assumption that at 300 K the effective mass does not depend on charge carrier concentration was invoked.

With a knowledge of $\eta$, one can use the Wiedemann-Franz relation to determine crystal thermal conductivity component due to free charge carriers:

$$\kappa_{n,p(mono)} = L\sigma T. \tag{9}$$

In so doing, the Lorentz number is equal to:

$$L = \left(\frac{k_B}{e}\right)^2 \left[\frac{3F_2(\eta)}{F_0(\eta)} - \frac{4F_1^2(\eta)}{F_0^2(\eta)}\right]. \tag{10}$$

Knowing the thermal conductivity due to free carriers, as well as the experimental thermal conductivity of TEM described by corresponding approximation model, one can readily determine its lattice component. Knowing the temperature and concentration dependence of the lattice component of the thermal conductivity of TEM, it is easy, using the method developed in [8] with regard to relations given in [11], to determine coefficient $\mu$ of polynomials (3), (4) characterizing frequency dependence of phonon-phonon scattering probability.

## The results of optimization of materials for coolers

Calculation of dependences of the figure of merit of microlayers on the concentration of charge carriers was performed for *n*-type materials $Bi_2Te_{2.7}Se_{0.3}$ + (0.09…0.03) % $CdCl_2$ and

*p*-type materials $Bi_{0.5}Sb_{1.5}Te_3 + 4\ \%\ Te$ which are used for cooling modules. We employed the averaged experimental dependences given in [6, 9] of the kinetic coefficients $\alpha_{mono}$, $\sigma_{mono}$, $\kappa_{mono}$ of these materials on the temperature and electrical conductivity values at 300 K, proportional to charge carrier concentration. The calculations used parameters of phonon spectra and density-of-state effective masses of electrons and holes given in [12]. The calculations were performed on the basis of relations (1) – (4) by computer methods in the Mathcad-14 environment.

The concentration dependences of the figure of merit *ZT* of thin layers obtained for various thicknesses and temperatures are given in Fig. 1 – 6.

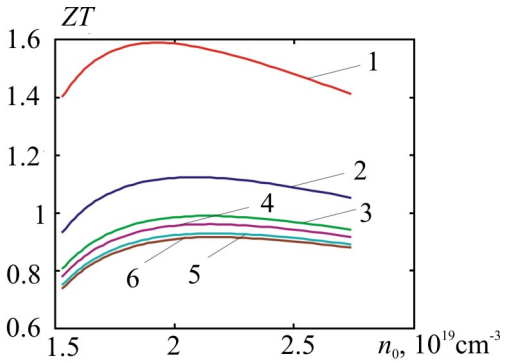


*Fig. 1. Concentration dependences of ZT of thin layers of n-type TEM $Bi_2Te_{2.7}Se_{0.3}$ at temperature 300 K and layer thicknesses, μm: 1 – 0.1; 2 – 1; 3 – 5; 4 – 10; 5 – 50; 6 – bulk crystal.*

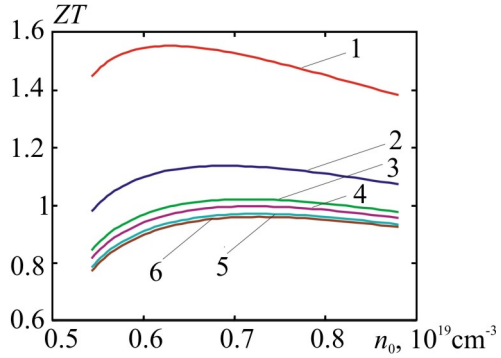


*Fig. 2. Concentration dependences of ZT of thin layers of p-type TEM $Bi_{0.5}Sb_{1.5}Te_3$ at temperature 300 K and layer thicknesses, μm: 1 – 0.1; 2 – 1; 3 – 5; 4 – 10; 5 – 50; 6 – bulk crystal.*

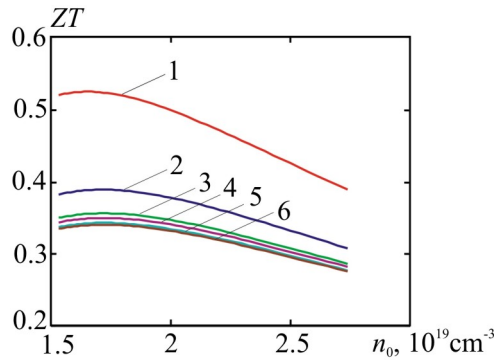


*Fig. 3. Concentration dependences of ZT of thin layers of n-type TEM $Bi_2Te_{2.7}Se_{0.3}$ at temperature 150 K and layer thicknesses, μm: 1 – 0.1; 2 – 1; 3 – 5; 4 – 10; 5 – 50; 6 – bulk crystal.*

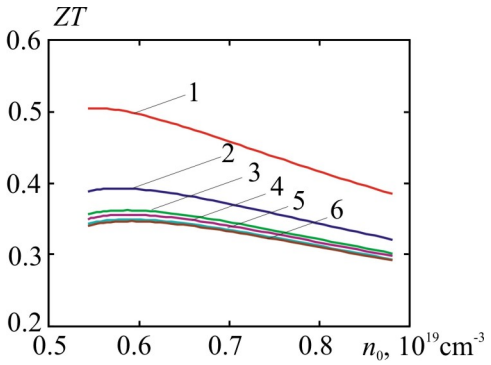


*Fig. 4. Concentration dependences of ZT of thin layers of p-type TEM $Bi_{0.5}Sb_{1.5}Te_3$ at temperature 150 K and layer thicknesses, μm: 1 – 0.1; 2 – 1; 3 – 5; 4 – 10; 5 – 50; 6 – bulk crystal.*

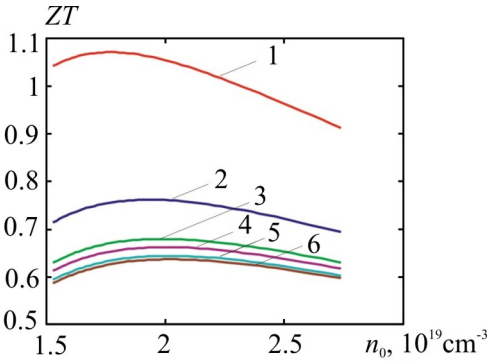


*Fig. 5. Concentration dependences of ZT of thin layers of n-type TEM $Bi_2Te_{2.7}Se_{0.3}$ at temperature 225 K and layer thicknesses, μm: 1 – 0.1; 2 – 1; 3 – 5; 4 – 10; 5 – 50; 6 – bulk crystal.*

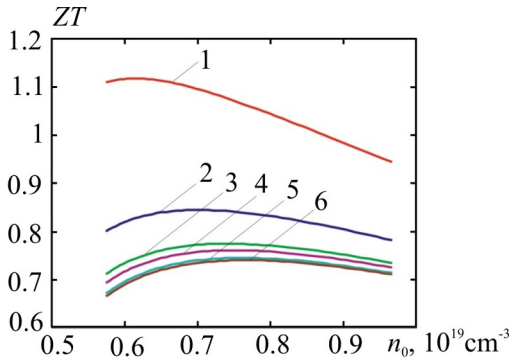


*Fig. 6. Concentration dependences of ZT of thin layers of p-type TEM $Bi_{0.5}Sb_{1.5}Te_3$ at temperature 225 K and layer thicknesses, μm: 1 – 0.1; 2 – 1; 3 – 5; 4 – 10; 5 – 50; 6 – bulk crystal.*

From the figures it is seen that for the above materials at all temperatures when passing from single crystal to thin TEM layers there is a gain in the figure of merit. The figure of merit enhancement is attributable to the impact of size effects related to compatibility of charge carrier and phonon mean free paths to layer thicknesses. In all cases there is thickness-dependent optimal concentration of charge carriers whereby maximum thermoelectric figure of merit is achieved. However, as long as charge carrier and phonon mean free paths are measured by nanometers, there is no essential gain in the thermoelectric figure of merit when passing from single crystal to layers 50 μm thick. Essential gain, namely by a factor of 1.2 – 2 as compared to single crystal, is

obtained in the range of thicknesses 0.1 – 1 μm. Nevertheless, the results imply that transition from a single crystal to thin layers can be done without degrading the output parameters of coolers, and hence, one can achieve substantial saving of TEM. To achieve a more essential gain in the figure of merit, one must pass to still thinner, e.g. submicron layers or nanolayers. However, a gain in the figure of merit with such thin TEM can be assured and maintained only using special technology of creating TEM-metal contacts providing possibly lower values of contact resistances.

## Results of optimization of materials for generators

Calculation of dependences of the figure of merit of microlayers on the concentration of charge carriers was performed for *n*-type materials $(Bi_2Te_3)_{0.9}(Sb_2Te_3)_{0.05}(Sbi_2Se_3)_{0.05}$ and *p*-type materials $(Bi_2Te_3)_{0.25}(Sb_2Te_3)_{0.72}(Sb_2Se_3)_{0.03}$ which are used for generator modules. The averaged experimental dependences given in [9] of the kinetic coefficients $\alpha_{mono}$, $\sigma_{mono}$, $\kappa_{mono}$ of these materials on temperature and the electrical conductivity values at 300 K were employed. The calculations used parameters of phonon spectra and density-of-state effective masses of electrons and holes given in [10, 13].

The concentration dependences of the figure of merit *ZT* of thin layers of these materials obtained for various thicknesses and temperatures are given in Fig. 7 – 12.

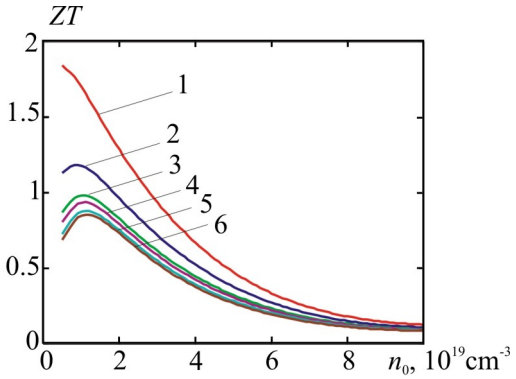


*Fig. 7. Concentration dependences of ZT of thin layers of n-type TEM $(Bi_2Te_3)_{0.9}(Sb_2Te_3)_{0.05}(Sb_2Se_3)_{0.05}$ at temperature 300 K and layer thicknesses, μm: 1 – 0.1; 2 – 1; 3 – 5; 4 – 10; 5 – 50; 6 – bulk crystal.*

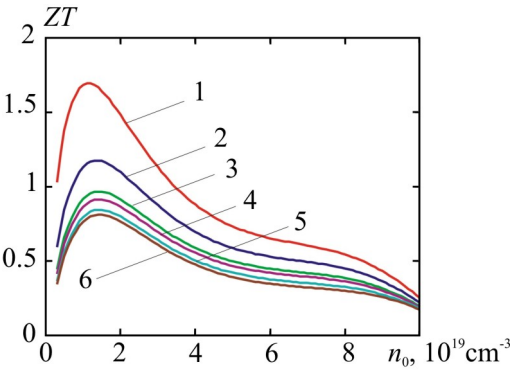


*Fig. 8. Concentration dependences of ZT of thin layers of p-type TEM $(Bi_2Te_3)_{0.25}(Sb_2Te_3)_{0.72}(Sb_2Se_3)_{0.03}$ at temperature 300 K and layer thicknesses, μm: 1 – 0.1; 2 – 1; 3 – 5; 4 – 10; 5 – 50; 6 – bulk crystal.*

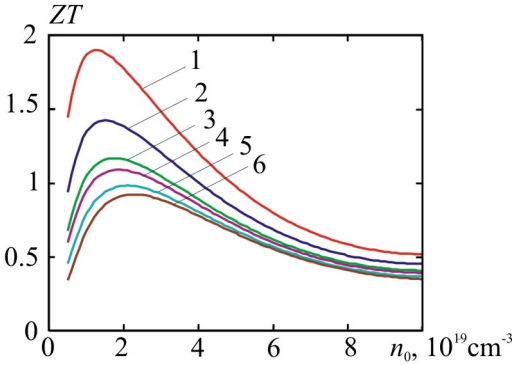


*Fig. 9. Concentration dependences of ZT of thin layers of n-type TEM $(Bi_2Te_3)_{0.9}(Sb_2Te_3)_{0.05}(Sb_2Se_3)_{0.05}$ at temperature 450 K and layer thicknesses, μm: 1 – 0.1; 2 – 1; 3 – 5; 4 – 10; 5 – 50; 6 – bulk crystal.*

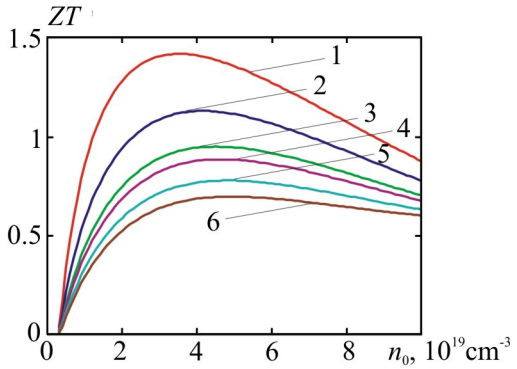


*Fig. 10. Concentration dependences of ZT of thin layers of p-type TEM $(Bi_2Te_3)_{0.25}(Sb_2Te_3)_{0.72}(Sb_2Se_3)_{0.03}$ at temperature 450 K and layer thicknesses, μm: 1 – 0.1; 2 – 1; 3 – 5; 4 – 10; 5 – 50; 6 – bulk crystal.*

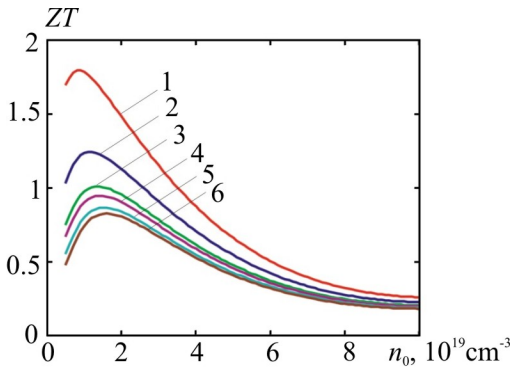


*Fig. 11. Concentration dependences of ZT of thin layers of m-type TEM $(Bi_2Te_3)_{0.9}(Sb_2Te_3)_{0.05}(Sb_2Se_3)_{0.05}$ at temperature 375 K and layer thicknesses, μm: 1 – 0.1; 2 – 1; 3 – 5; 4 – 10; 5 – 50; 6 – bulk crystal.*

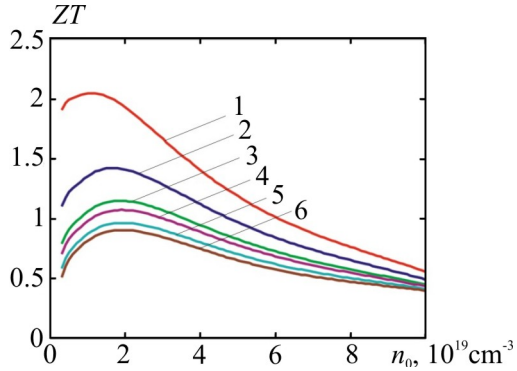


*Fig. 12. Concentration dependences of ZT of thin layers of p-type TEM $(Bi_2Te_3)_{0.25}(Sb_2Te_3)_{0.72}(Sb_2Se_3)_{0.03}$ at temperature 225 K and layer thicknesses, μm: 1 – 0.1; 2 – 1; 3 – 5; 4 – 10; 5 – 50; 6 – bulk crystal.*

Just as in the case of materials for coolers, for each thickness of TEM layer there is optimal concentration of charge carriers whereby maximum thermoelectric figure of merit is achieved, and in the case of materials for generators it is expressed stronger than in the case of materials for coolers. Essential gain in the thermoelectric figure of merit, namely by a factor of 1.6 – 3.2 as compared to single crystal is obtained in the range of thicknesses 0.1 – 1 μm. At thicknesses 1 – 50 μm the gain is reduced, though it makes about 4 % as compared to single crystal.

There is no need in additional optimization of the figure of merit of materials for the concentration of doping impurities as compared to single crystal in the range of thicknesses 5 – 50 μm. Some change in concentration is required only at thicknesses 0.1 μm. In particular, it must be reduced by a factor of 1.14 – 2.2 as compared to single crystal. The strongest change is required for *n*-type generator materials.

## Conclusions

1. The impact of phonon and charge carrier scattering at the boundaries of microminiature TEM layers on the electrical conductivity and lattice thermal conductivity is the most essential factor assuring thermoelectric figure of merit when passing from single crystal to layers of thickness from 50 μm. The figure of merit improvement can be expected at lower layer thicknesses.
2. The use of thin TEM layers instead of single crystals allows for essential saving of TEM without sacrificing the output parameters and characteristics of thermoelectric coolers and generators.
3. A stronger reduction of lattice thermal conductivity as compared to electrical conductivity creates opportunities for TEM figure of merit improvement when passing from the bulk single crystals to microminiature layers.
4. The greatest gain in the figure of merit, namely 1.7 – fold for cooling materials and 3.15 – fold for generator materials is achieved at layer thickness 0.1 μm.
5. At thicknesses over 50 μm and temperatures 150 – 300 K the expected improvement of the figure of merit of considered materials with respect to corresponding single crystals does not exceed 4 %.

## References

1. N.S.Lidorenko, V.A.Andriyako, L.D.Dudkin, and E.L.Nagayev, The Effect of Tunneling on the Efficiency of Thermoelectric Devices, *Doklady Akademii Nauk SSSR* 1295 (1969).
2. A.D.Terekhov, E.M.Sher, Structure of Dispersion and the Effective Values of Thermal Conductivity and Electric Conductivity Coefficients, in: *"Thermoelectric Materials and Films. Materials of All-Union Conference on the Deformation and Size Effects in Thermoelectric Materials and Films, Technology and Application of Films"* (Leningrad, 1976), p.211.

3. L.P.Bulat, I.A.Drabkin, V.V.Karatayev, V.B.Osvensky, and A.I.Sorokin, Effect of Scattering on the Boundaries on the Thermal Conductivity of Nanostructured Semiconductor Material $Bi_xSb_{2-x}Te_3$, *Physics of the Solid State* 52, 1712 – 1716 (2010).
4. M.S.Dresselhaus, G. Dresselhaus, X.Sun, Z.Zhang, S.B.Kronin, and T.Koga, *Physics of the Solid State* **41**(5), 755 – 758 (1999).
5. L.I.Anatychuk, P.V.Gorskiy, and V.P. Mikhalchenko, Impact of Size Effects on the Properties of Thermoelectric Materials, *J.Thermoelectricity* 1, 5 – 13 (2014).
6. L.I.Anatychuk, *Thermoelements and Thermoelectric Devices. Handbook* (Kyiv: Naukova Dumka, 1976), 726p.
7. P.V.Gorskiy, V.P.Mikhalchenko, Reduction of Thermoelectric Material Lattice Thermal Conductivity Using Shape-Forming Element Optimization, *J.Thermoelectricity* 1, 19 – 27 (2013).
8. P.V.Gorskiy, V.P.Mikhalchenko, On the Electric Conductivity of Contacting Particles of Thermoelectric Material, *J.Thermoelectricity* 2, 12 – 18 (2013).
9. L.I.Anatychuk, L.N.Vikhor, *Functionally Graded Thermoelectric Materials* (Institute of Thermoelectricity: Kyiv-Chernivtsi, 2012), 180p.
10. B.M.Goltsman, V.A.Kudinov, and I.A.Smirnov, *Semiconductor Thermoelectric Materials Based on* $Bi_2Te_3$ (Moscow: Nauka, 1972), 320p.
11. P.G.Klemens, Lattice Thermal Conductivity, In: *Solid State Physics. Advances in Research and Applications, Vol.7, 1 – 98* (Academic Press. Inc. Publishers, New York, 1958), 526 p.
12. L.W.Da Silva, M.Kaviany, Micro-Thermoelectric Cooler: Interfacial Effect on Thermal and Electrical Transport, *Int. J. Heat and Mass Transfer* 478, 2417 – 2435 (2004).
13. *CRC Handbook of Thermoelectrics, edited by D.M.Rowe* (CRC Press, London, New York, 1995).

Submitted 07.10.2015

*Yu.A. Kruglyak*

**Yu.A. Kruglyak**

Department of Information Technologies, Odessa
State Environmental University,
Lvivska Str. 15, Odessa, 65016, Ukraine

# THERMOELECTRIC PHENOMENA IN "BOTTOM – UP" APPROACH

*Thermoelectric phenomena of Seebeck and Peltier, quality indices of thermoelectric devices and materials and thermoelectric optimization, ballistic and diffusive transport of phonons and its role in the thermal conductivity are discussed in the frame of the «bottom – up» approach of modern nanoelectronics.*

**Key words:** nanoelectronics, microelectronics, electron conductivity modes, phonon conductivity modes, Seebeck effect, Peltier effect, power factor, *ZT* product, thermoelectric optimization.

## Introduction

Both previous publications [1, 2] have been devoted to modern Landauer – Datta – Lundstrom (LDL) electron and heat transport model [3 – 7] which works well at the nanoscale as well as at macroscale for 1D, 2D, and 3D resistors in ballistic, quasi-ballistic, and diffusive linear response regimes when there may be differences in both voltage and temperature across the device. Success of the LDL transport model is associated primarily with the use of the "bottom – up" approach when discussing different topics in electronics in contrary to historically traditional "top – down" approach [8 – 11].

We seek today to bring a new perspective to university and engineering education to meet the challenges and opportunities of modern nanotechnology. Sixty years ago electronics faced a similar challenge brought on by the advent of the transistor and it was met effectively: a generation of physicists and engineers ready to lead the modern electronics industry has been trained.

Today we face the need for a comparable revolution in education as well as in research. Ever since the birth of solid state physics, materials have been described in terms of average material parameters like the mobility or the optical absorption coefficient which are then used as inputs to macroscopic device models. This "top – down" approach is being widely used even for modern nanostructured materials, but we believe that it is no longer adequate to meet the challenges and opportunities of our day. An integrated approach is needed that embeds new ways of thinking, emerging from current research on nanoscience, directly into the models used for non-equilibrium problems like nanoscale transistors, energy conversion devices and bio-sensors. This new "bottom – up" approach to electronic devices and materials is being most successfully demonstrated in the

Network of Computational Nanotechnology at Purdue University, USA [12]. In this paper we discuss thermoelectric phenomena in the "bottom – up" approach partly following lecture course "Fundamentals of Nanoelectronics: Basic Concepts" given by Supriyo Datta in 2012 [13].

Conduction measurements themselves do not tell us anything about the nature of the conduction process inside the conductor. In the closed circuit, electrons always move from the negatively charged contact through conductor to the positively charged contact whatever the physical and chemical nature of the conductor. This is true for all conductors and therefore conductivity measurements do not tell us anything about the conductor itself.

On the other hand, thermoelectric phenomena as those where current is generated by the temperature difference on the conductor contacts, provide the opportunity to judge on the physical nature of the conductivity. The simplest examples are the conductors of *n*- and *p*-type. In the *n*-type conductors, electrons move from the hot contact through conductor to the cold one, but in the *p*-type conductors the direction of electron transport is opposite. Why?

It is often explained that *p*-conductors show the opposite effect due to the carriers (so called "holes") having the opposite sign relative to electrons moving in the *n*-conductors. However, this explanation is not quite satisfactory since what actually move are electrons with a negative charge. "Holes" are at the best a conceptual convenience and experimental effects observed in the laboratory should not depend on the subjective conveniences.

Differences between *n*- and *p*-conductors are best explained in the "bottom – up" approach [13 – 17]. In *n*-conductors the density-of-states $D(E)$ increases with increasing energy $E$, while in the *p*-conductors it decreases with increasing $E$. In the *n*-type conductors the electrochemical potential $E_F$ is located near the bottom of a band of energies, while in the *p*-type conductors it is located near the top. In the last case the flow of electrons happens near the top of a band of energies and it is just convenient to keep track of the empty states above $E_F$ rather than the filled states below $E_F$. These empty states are called holes and since they represent the absence of an electron they behave like positively charged entities.

Differences between *n*- and *p*-conductors do not require new principles or assumptions beyond what we have already discussed [1, 2], namely: electric current is driven by the difference between Fermi functions on contacts of the conductor $f_1(E) - f_2(E)$.

Another important physical phenomenon is known, called the Hall effect, which changes sign for the *n*- and *p*-types conductors and the Hall effect too is commonly blamed for negatively charged electrons and positively charged "holes". The Hall effect, however, has a totally different origin related to the negative mass associated with $E(p)$ relations in *p*-conductors that points downwards [18]. By contrast the thermoelectric phenomena do not require a conductor to even have a $E(p)$ relation. Even small molecules show sensible thermoelectric effects [19 – 21]. Molecular junctions hold significant promise for efficient and high-power-output thermoelectric energy conversion.

To explain differences between *n*- and *p*-conductors in the "bottom – up" approach, let us

remind well known now expression for current through an elastic resistor (32) in [14]:

$$I = \frac{1}{q}\int_{-\infty}^{+\infty} dE G(E)\left(f_1(E) - f_2(E)\right), \tag{1}$$

where $G(E)$ is the conductivity. If previously [14] the difference between the Fermi functions was generated by the difference between the electrochemical potentials at the same temperature of the contacts, the difference as well can be generated by the difference in temperature of contacts since the Fermi functions depend on both $E_F$ and $T$, namely:

$$f_1(E) = 1/(e^{(E-E_{F_1})/kT_1} + 1) \tag{2a}$$

and

$$f_2(E) = 1/(e^{(E-E_{F_2})/kT_2} + 1). \tag{2b}$$

Why with the temperature difference between contacts the direction of current is opposite in *n*- and *p*-type conductors? The reason lies in the behavior of the difference of the Fermi functions of hot and cold contacts (Fig. 1).

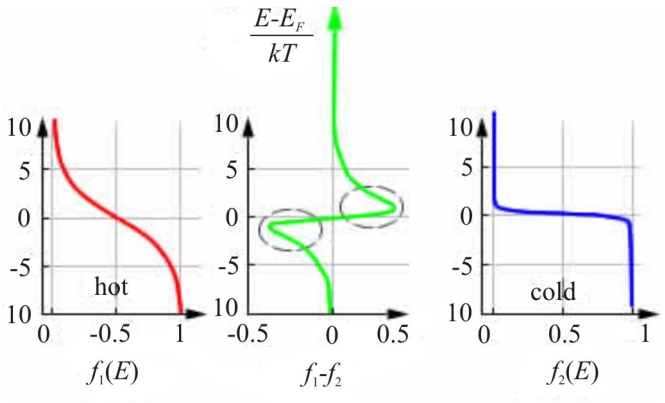


*Fig. 1. Two contacts, hot and cold, with the same value of $E_F$: the difference of the Fermi functions is positive for $E > E_F$ and negative for $E < E_F$.*

In the *n*-type channel conductivity $G(E)$ is the increasing function of energy, so that the states with $E > E_F$ dominate in the total current, the electrons move from the left contact to the right one, from hot to cold (Fig. 2).

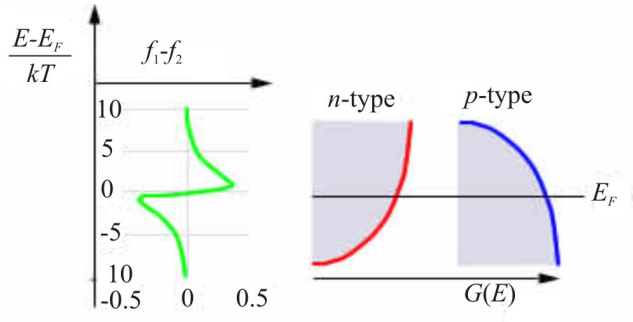


*Fig. 2. For the n-conductor the current for $E > E_F$ dominates the current for $E < E_F$, while for p-conductors situation is opposite − the current for $E < E_F$ dominates the current for $E > E_F$.*

Situation is opposite in the *p*-channels. Conductivity $G(E)$ is the decreasing function of energy, so that the states with $E < E_F$ dominate in the total current, the electrons move from the right contact to the left one, from cold to hot (Fig. 2).

Consequently, electrons flow from hot to cold across the *n*-type resistor, but from cold to hot in a *p*-type channel. Exactly this explanation of the different behavior of *n*- and *p*-thermics in the "bottom – up" approach is used in the LDL transport model [22, 23].

### Seebeck coefficient

To calculate the current due to the difference in the temperature of contacts, one can use eqn (1) directly, without introducing any simplifications. However, in the case of small differences in the temperature of contacts, as has been already demonstrated in the case of the small difference between the electrochemical potentials in [1, 7, 14, 15], which corresponds to the low bias or linear response regime, you can use the decomposition of the difference of the Fermi functions in (1) in the Taylor series and limit itself by the linear term. Then we can write

$$I = G(V_1 - V_2) + G_S(T_1 - T_2). \tag{3}$$

This shows that the electrons move from the hot contact through the *n*-conductor to the cold contact, and in the *p*-conductors the direction of transport is opposite. Let us rewrite (3) as

$$\Delta V = \frac{I}{G} + \left(-\frac{G_S}{G}\right)\Delta T, \tag{4}$$

where $V_1$ and $V_2$ are defined as $E_{F_1}/q$ and $E_{F_2}/q$, and the conductance $G$ is given by [1]

$$G = \int_{-\infty}^{+\infty} dE\, G(E)\left(\frac{\partial f_0}{\partial E_F}\right) = \int_{-\infty}^{+\infty} dE\left(-\frac{\partial f_0}{\partial E}\right)G(E), \tag{5}$$

whereas the Seebeck conductivity

$$G_S = \frac{1}{q}\int_{-\infty}^{+\infty} dE\, G(E)\left(\frac{\partial f_0}{\partial T}\right) = \int_{-\infty}^{+\infty} dE\left(-\frac{\partial f_0}{\partial E}\right)\frac{E - E_{F_0}}{qT}\, G(E). \tag{6}$$

The Seebeck coefficient *S* is defined as the ratio of these two conductivities:

$$S = -G_S/G. \tag{7}$$

Equation (6) mathematically expresses the fact that the states with energy higher and lower of the electrochemical potential, contribute to the thermoelectric Seebeck coefficient *S* with different signs. From this equation it is clear that selecting the material with the best Seebeck coefficient one should choose such a material in which all the state density is concentrated on one side of the electrochemical potential $E_{F_0}$, since even the small fraction of the states on the other side of $E_{F_0}$ only brings the Seebeck coefficient down.

Relations (3) and (4) may be illustrated by the two circuits (Fig. 3): short circuit with current

$$I_{sc} = G_S\left(T_1 - T_2\right) \tag{8}$$

and open circuit, which is usually used in thermoelectric power measurements giving voltage

$$V_{oc} = -\frac{I_{sc}}{G} = -\frac{G_S}{G}\left(T_1 - T_2\right). \tag{9}$$

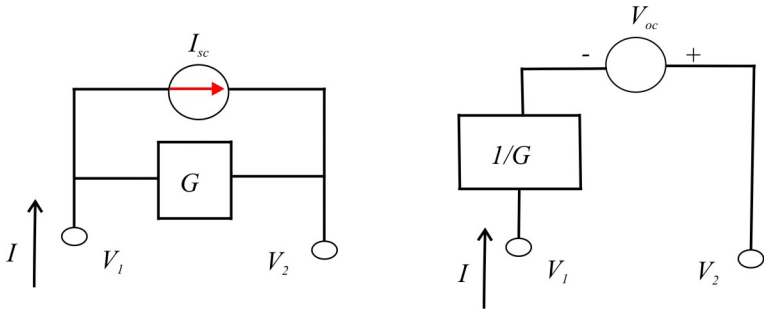


*Fig. 3. Short circuit (sc) and open circuit (oc) illustrating the eqns (3) and (4). For the direction of current (the same as the direction of electron flow) and for the voltage sign the natural conditions are used, which are opposite to the ones traditionally used.*

For example, for the *n*-conductors the Seebeck conductivity is positive, thus the voltage $V_{oc}$ is negative if $T_1 > T_2$. This means that contact with the higher temperature is charged negatively (positive in the conventional sense). According to agreement, the Seebeck coefficient

$$S \equiv \frac{V_{oc}}{T_1 - T_2} = -\frac{G_S}{G}. \tag{10}$$

## Quality indices of thermoelectric devices and materials

In practical applications the thermoelectric effect is interesting in a sense that the heat excess can be converted into electricity [24]. Maximum of power $P$ is generated when the loaded resistance $R_L = 1/G$, namely:

$$P_{max} = V_{oc}^2 G/4 = S^2 G\left(T_1 - T_2\right)^2/4, \tag{11}$$

where $S^2G$ is known as the power factor and is one of the standard figures of merit for thermics.

The ratio of the maximum generated power to the power that is supplied by the external source is a good measure of the efficiency of the thermoelectric material in converting heat to electricity and is called the coefficient of performance

$$\eta \equiv \frac{P_{max}}{G_K\left(T_1 - T_2\right)} = \frac{S^2 GT}{G_K}\frac{T_1 - T_2}{4T}, \tag{12}$$

where $G_K$ − the thermoconductivity of the material, and $T$ is the mean temperature $(T_1 + T_2)/2$. The standard figure of merit for thermics, called its $ZT$ product is proportional to the ratio of $S^2G$ to $G_K$:

$$ZT \equiv \frac{S^2GT}{G_K} = \frac{S^2\sigma T}{k}, \tag{13}$$

where the specific thermal conductivity $k$ is related to the thermal conductivity $G_K$ of the conductor material

$$G_K = k \cdot A / L \tag{14}$$

as the electric conductivity is related to the specific conductivity of the conductor of length $L$ with cross-sectional area $A$. Fourier law for the thermoconduction, the analog of the Ω law for the electrical conductivity, when applied to nanoresistors, needs the same correction ($L \Rightarrow L + \lambda$) as the Ω law [7, 14].

The electrical conductivity arises solely from electrons. The thermal conductivity includes also a contribution of phonons. Usually it is the phonon component that dominates the thermal conductivity. It will be discussed a bit later. For now we shall discuss the heat carried by electrons only.

## Heat current

So far, we have discussed the thermoelectric conductivity of a material with any arbitrary conductance $G(E)$. Model of the elastic resistor [14, 15] is attractive in a sense that modes at different energies all conduct in parallel, so that we can consider the conductivity at a certain value of the energy, and then just sum up over the entire spectrum of energies. Consider a small energy range between $E$ and $E + dE$ located either above the value of the electrochemical potential $E_{F_0}$ ($n$-type modes) or below ($p$-type modes) (Fig. 4). As it was mentioned above, the contributions of these two different types of modes into Seebeck effect are opposite in sign.

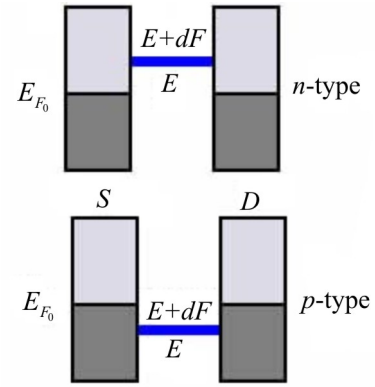


*Fig. 4. The simplest single-mode conductance G(E) with the conductance mode between energies E and E + dE (dE << kT) above (n-type mode) and lower (p-type mode) of the electrochemical potential.*

When there is a current in the elastic resistor the Joule heat $I^2R$ is dissipated at the contacts of the conductor with the source $S$ and drain $D$ [14, 15]. In channels of the $n$- and $p$-type in Fig. 4

heat is not released at the contacts, since there is no current in the channels (there is the same electrochemical potential at the *S* and *D*). Let us now consider the situation in Fig. 5 with different electrochemical potentials at the *S* and *D*, which corresponds, for example, to the contact between two different metals. Every time when an electron is transferred from *S* to *D* through the *n*-type mode the source is cooled, and the drain is heated, and it is in contrary for the *p*-type mode − the source is heated, and the drain is cooled (Peltier effect), but each time the cumulative effect is $E_{F_1} - E_{F_2} = qV$ with the Joule heating.

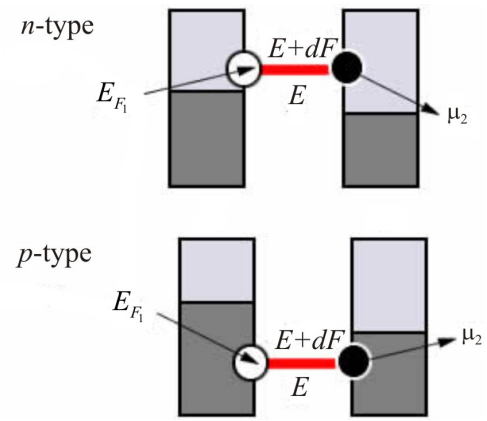


*Fig. 5. Contact of two metals with different electrochemical potentials (Peltier effect).*

The charge current *I* is given by eqn (1). Keeping in mind that in the window $E_{F_1} - E_{F_2}$ an electron loses energy $E - E_{F_1}$ on *S* and gains the energy $E - E_{F_2}$ on *D*, we can write the thermoelectric energy contributions separately for the *S* and *D*, namely:

$$I_{Q_1} = \frac{1}{q}\int_{-\infty}^{+\infty} dE \frac{E - E_{F_1}}{q} G(E)\left(f_1(E) - f_2(E)\right) \tag{15}$$

and

$$I_{Q_2} = \frac{1}{q}\int_{-\infty}^{+\infty} dE \frac{E_{F_2} - E}{q} G(E)\left(f_1(E) - f_2(E)\right). \tag{16}$$

Energy extracted from an external source

$$I_{ext} = \frac{E_{F_1} - E_{F_2}}{q} I = VI, \tag{17}$$

thus the energy conservation law is satisfied:

$$I_{Q_1} + I_{Q_2} + I_{ext} = 0. \tag{18}$$

**Linear response**

Lets linearize eqs (15) and (16) in the same way as we have obtained eqn (3) from eqn (1) and will get

$$I_Q = G_P(V_1 - V_2) + G_Q\left(T_1 - T_2\right), \tag{19}$$

where

$$G_P = \int_{-\infty}^{+\infty} dE\left(-\frac{\partial f_0}{\partial E}\right)\frac{E - E_{F_0}}{q}G\left(E\right) \tag{20}$$

and

$$G_Q = \int_{-\infty}^{+\infty} dE\left(-\frac{\partial f_0}{\partial E}\right)\frac{\left(E - E_{F_0}\right)^2}{q^2 T}G\left(E\right) \tag{21}$$

are the standard expressions for the thermoelectric coefficients, which are usually obtained by using of such sophisticated approaches as the Boltzmann transport equation technique [5] or Kubo formalism [6]. We are still talking about electronic contributions to the thermoelectric coefficients.

It should be remembered that the value $G_Q$ is not the thermoconductivity $G_K$ of the conductor material commonly used in the standard figure of merit $ZT$ (13). One reason for this, as already mentioned, is that in the thermoconductivity $G_K$ there is the phonon contribution, which has not yet been taken into account. But there is one more, very different reason.

Value $G_K$ is defined as the thermal conductivity of the resistor under the open circuit conditions ($I = 0$)

$$G_K = \left(\frac{\partial I_Q}{\partial\left(T_1 - T_2\right)}\right)_{I=0}, \tag{22}$$

whereas the value of $G_Q$ is the thermal conductivity of the resistor under the short circuit conditions ($V = 0$; $V_1 = V_2$)

$$G_Q = \left(\frac{\partial I_Q}{\partial\left(T_1 - T_2\right)}\right)_{V_1=V_2}. \tag{23}$$

However, we can rewrite eqs (3) and (19) in such a way as to give us the open circuit coefficients, namely:

$$\left(V_1 - V_2\right) = \frac{1}{G}I - \frac{G_S}{G}\left(T_1 - T_2\right), \tag{24}$$

$$I_Q = \frac{G_P}{G}I + \left(G_Q - \frac{G_P G_S}{G}\right)\left(T_1 - T_2\right) \tag{25}$$

with notification, of course, as mentioned earlier, that $V$ and $I$ represent the voltage $E_F/q$ and electron current, which are opposite in sign to the conventional agreement about voltage and current, where $-G_S/G$ is the Seebeck coefficient (10), the Peltier coefficient

$$\Pi = -G_P/G \tag{26}$$

and the thermal conductivity

$$G_K = G_Q - G_P G_S / G \,. \tag{27}$$

Using the eqs (6) and (20), the Seebeck and Peltier coefficients in eqs (24) and (25) are related by the Kelvin relation

$$\Pi = TS \,, \tag{28}$$

which is the special case of the fundamental Onsager relations [27].

## Delta thermoelectrics

It is useful to look at a so called delta-function thermoelectric, which is considered to be a hypothetical material with a narrow conductance mode at energy ε with a width $\Delta\varepsilon << kT$, and calculate its thermoelectric coefficients (Fig. 6).

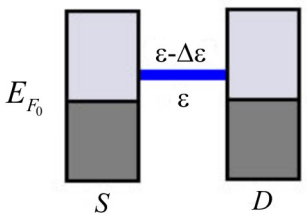


*Fig. 6. Model of the delta thermoelectrics.*

Let us first recall general definitions for thermoelectric coefficients obtained so far:

$$G = \int_{-\infty}^{+\infty} dE \left( -\frac{\partial f_0}{\partial E} \right) G(E), \quad G_S = \int_{-\infty}^{+\infty} dE \left( -\frac{\partial f_0}{\partial E} \right) \frac{E - E_{F_0}}{qT} G(E),$$

$$G_P = \int_{-\infty}^{+\infty} dE \left( -\frac{\partial f_0}{\partial E} \right) \frac{E - E_{F_0}}{q} G(E), \; G_Q = \int_{-\infty}^{+\infty} dE \left( -\frac{\partial f_0}{\partial E} \right) \frac{\left( E - E_{F_0} \right)^2}{q^2 T} G(E).$$

Conductivity $G(E)$ in the integrand is different from zero in the very narrow range of energy and the factors $\left( E - E_{F_0} \right)$ are practically constant and can be pulled out of the integrals, thus giving

$$G = G(\varepsilon) \Delta\varepsilon \left( -\frac{\partial f_0}{\partial E} \right)_{E=\varepsilon}, \tag{29}$$

$$G_S = \frac{\varepsilon - E_{F_0}}{qT} G, \tag{30}$$

$$G_P = \frac{\varepsilon - E_{F_0}}{q} G, \tag{31}$$

$$G_Q = \frac{\left(\varepsilon - E_{F_0}\right)^2}{q^2 T} G. \tag{32}$$

Using (24) and (25) it is now easily to obtain the thermoelectric coefficients for the delta-thermoelectrics:

$$S = -\frac{G_S}{G} = -\frac{\varepsilon - E_{F_0}}{qT}, \tag{33}$$

$$\Pi = -\frac{G_P}{G} = -\frac{\varepsilon - E_{F_0}}{q}, \tag{34}$$

$$G_K = G_0 - \frac{G_P G_S}{G} = 0. \tag{35}$$

Zero conductivity $G_K$ for the delta thermoelectrics deserves discussion. First, however, we shall consider the physical meaning of the Seebeck (33) and Peltier (34) coefficients for the delta thermoelectrics. The Seebeck coefficient (33) is the open circuit voltage required to maintain zero current. The delta-thermoelectrics conduct only when energy $E = \varepsilon$. In order to have no current, the Fermi functions at this energy should be the same: $f_1(\varepsilon) = f_2(\varepsilon)$, which in turn gives

$$\frac{\varepsilon - E_{F_1}}{kT_1} = \frac{\varepsilon - E_{F_2}}{kT_2} = \frac{\left(\varepsilon - E_{F_1}\right) - \left(\varepsilon - E_{F_2}\right)}{k\left(T_1 - T_2\right)} = -\frac{E_{F_1} - E_{F_2}}{k\left(T_1 - T_2\right)}. \tag{36}$$

Since the Seebeck coefficient at zero current is defined as

$$S = \frac{\left(E_{F_1} - E_{F_2}\right)/q}{T_1 - T_2}, \quad (I = 0) \tag{37}$$

we finally get

$$S = -\frac{\varepsilon - E_{F_1}}{qT_1} = -\frac{\varepsilon - E_{F_2}}{qT_2} = -\frac{\varepsilon - E_{F_0}}{qT}, \tag{38}$$

which is consistent with the earlier expression (33).

Expression (34) for the Peltier coefficient of the delta-thermoelectrics also easy to understand if you remember that each electron in the delta-thermoelectrics carries heat $\varepsilon - E_{F_0}$, so that the ratio of the transferred heat to the charge of the electron $(-q)$ should be $(\varepsilon - E_{F_0})/(-q)$.

As a result, there is zero thermal conductivity (35), which suggests that in the delta-thermoelectrics inder open circuit conditions (no electron transfer) the heat transfer does not occur. It seems to be so. However, after all if there is no electrical current, how can there be a heat current? If the delta-thermoelectric model would be sufficient to describe the realistic thermoelectrics, then no thermoelectric would have any heat conductance.

To understand the situation, we shall complicate the model and consider the two-level thermoelectric with the temperature difference (Fig. 7). In this case, under open circuit conditions there is a voltage between the two contacts with $E_{F_1} < E_{F_2}$. Although the total current is zero, but the individual currents are nonzero at different levels. They are equal in magnitude but opposite in direction, so that the total current is zero.

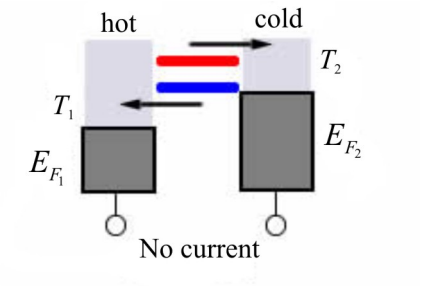


*Fig. 7. Two-level thermoelectric with temperature differences under open circuit conditions.*

However, the heat fluxes at both levels do not compensate each other because more heat is transferred on the level with higher energy than on the level with lower energy. Thus, the zero electric current does not guarantee the zero heat transfer in the real thermoelectrics, except that it takes place only in the delta-thermoelectrics.

Since the delta-thermoelectrics has zero thermoconductivity, its *ZT* product (13) must be very large with the claim to be the perfect thermoelectric. As mentioned above, even with the zero heat transfer by electrons the heat transfer by phonons takes place, which do not allows *ZT* product getting too large. We shall discuss the role of phonons later.

### Optimizing the power factor

Now we shall discuss the factors that could maximize the power factor $S^2G$ in expression (11) for the maximum power $P_{max}$. If you seek the maximum possible Seebeck coefficient, the energy ε in (33) must be chosen as far as possible from the chemical potential $E_{F_0}$. This, however, leads to the unacceptably low value of the conductance *G* (29), because the Fermi conductivity window $(-\partial f_0/\partial E)$ decays very rapidly as energy *E* moves away from $E_{F_0}$ [1, 7, 14].

From eqs (33) and (29) we have

$$S^2G = G(\varepsilon)\Delta\varepsilon\left(\frac{\varepsilon - E_{F_0}}{qT}\right)^2\left(-\frac{\partial f_0}{\partial E}\right)_{E=\varepsilon} = G(\varepsilon)\frac{\Delta\varepsilon}{kT}\left(\frac{k}{q}\right)^2 x^2\frac{e^x}{\left(e^x+1\right)^2}, \qquad (39)$$

where $x \equiv (\varepsilon - E_{F_0})/kT$, and the dependence of the power factor of *x* is given by the function $F(x) = x^2e^x/(e^x+1)^2$ with its graph shown in Fig. 8.

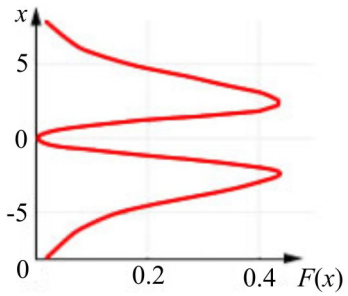


*Fig. 8. Graph of the function* $F(x) = x^2 e^x / (e^x + 1)^2$.

The function $F(x)$ has a maximum at $x \sim \pm 2$, suggesting that ideally one should place the mode energy approximately $2kT$ above or below the electrochemical potential $E_{F_0}$. The corresponding values of the Seebeck coefficient and the power factor is approximately equal

$$S \approx 2\frac{k}{q}, \tag{40}$$

$$S^2 G \approx 0.5\left(\frac{k}{q}\right)^2 G(\varepsilon)\frac{\Delta\varepsilon}{kT}. \tag{41}$$

The best thermoelectrics are characterized by the Seebeck coefficient, not much different from the value $2(k/q)$ = 170 μV/K, expected according eqn (40). They are usually designed in a way that the electrochemical potential $E_{F0}$ is located just below the conduction band, so that the product of $G(E)$ and $(-\partial f_0/\partial E)$ looks like the delta-function centered at $E = \varepsilon$ and lies just above the bottom of the conduction band as shown in Fig. 9.

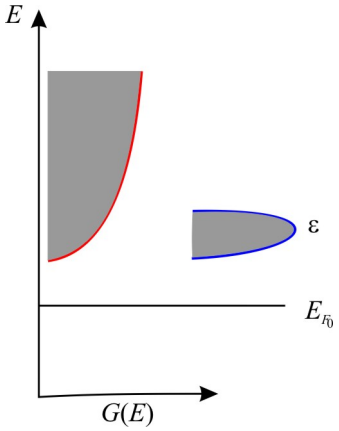


*Fig. 9. To design the best thermoelectrics.*

The problem, however, is that with such a design, the conductivity is not high enough, which it would be if the electrochemical potential $E_{F_0}$ would be situated higher, which is typical for metals. However, metals are poor thermoelectrics because their Seebeck coefficients are much smaller $k/q$, because their electrochemical potentials are closer to the middle of the band of states, so that there are as many states lie approximately above $E_{F_0}$ as well as below. For this

reason, the semiconductors dominate among good thermoelectrics, because they show the highest power factor. However, the power factor determines only the numerator of the *ZT* product (13). As already mentioned, the thermal conductivity in the denominator of eqn (13) depends strongly on the transport of heat by phonons, involving a physics that is quite different from a physics of the electron transport.

### Transport of heat by phonons

Phonon component, as is well known, along with the electronic component plays the extremely important role in the formation of the thermal properties of materials [24]. Without going into any detail of the physics of phonons [8 – 10, 28], we shall simply show how easily the model of electron transport [1, 14] can be rewritten for the phonons.

Unlike electrons, which obey Fermi statistics, the equilibrium distribution of phonons is described by the Bose function

$$n(\omega)=\frac{1}{\exp\left(\dfrac{\hbar\omega}{kT}\right)-1}. \tag{42}$$

The expression obtained in [1, 14] for the electric current

$$I=\frac{q}{h}\int_{-\infty}^{+\infty}dE\left(\frac{M\lambda}{L+\lambda}\right)_{el}\left(f_1(E)-f_2(E)\right), \tag{43}$$

where the Fermi functions (2) are written for the potential difference between the electrodes $V=(E_{F_1}-E_{F_2})/q$ and for different temperatures, $M$ − the number of the conduction modes, $L$ – resistor length, $\lambda$ is the mean-free-path for electrons, can be rewritten for the phonon heat flux

$$I_Q=\frac{1}{h}\int_{0}^{+\infty}d(\hbar\omega)\left(\frac{M\lambda}{L+\lambda}\right)_{ph}\hbar\omega\left(n_1(\omega)-n_2(\omega)\right) \tag{44}$$

simply by replacing $q\rightarrow\hbar\omega$, Fermi functions (2) to the Bose functions

$$n_1(\omega)=\frac{1}{\exp\left(\hbar\omega/kT_1\right)-1},\quad n_2(\omega)=\frac{1}{\exp\left(\hbar\omega/kT_2\right)-1} \tag{45}$$

and the lower limit of integration in (43) to zero.

Standard linearization [1, 14] of (44) gives

$$I_Q\approx G_K\left(T_1-T_2\right), \tag{46}$$

where the thermal conductance due to phonons can be written as

$$G_K=\frac{k^2T}{h}\int_{0}^{\infty}dx\left(\frac{M\lambda}{L+\lambda}\right)_{ph}\frac{x^2e^x}{\left(e^x-1\right)^2},\quad x\equiv\frac{\hbar\omega}{kT}. \tag{47}$$

Note that just as the model of the elastic resistor for electrons does not account for effects due to the inelastic scattering between the conduction modes, our phonon model ignores effects of the so called "anharmonic interactions" which causes phonons to convert from one frequency to another [29]. In contrast to the well-studied devices based on the electron ballistic transport, it is still little known about the devices based on the ballistic transport of phonons [30 – 32].

**Ballistic transport of phonons**

Ballistic phonon conductivity is usually written in the form resembling the Stefan-Boltzmann equation for photons.

From equation (47) for the ballistic conductivity ($L << \lambda$), we have

$$\left[G_K\right]_{bl} = \frac{k^2 T}{h}\int_0^\infty dx\, M_{ph}\frac{x^2 e^x}{\left(e^x - 1\right)^2}. \tag{48}$$

As for the case of electrons [14], the number of modes for the phonons:

$$M_{ph} = \frac{3\pi A}{\lambda_{ph}^2}, \tag{49}$$

where three allowed directions of phonon polarization had been taken into account and

$$\lambda_{ph} = \frac{c_s}{\omega/2\pi}, \tag{50}$$

where $c_s$ − the phonon velocity, so that

$$M_{ph} = \frac{3\omega^2 A}{4\pi c_s^2} = \frac{3k^2 T^2 A}{4\pi\hbar^2 c_s^2}x^2, \tag{51}$$

and finally from (48) we have

$$\left[G_K\right]_{bl} = \frac{3k^4 T^3}{8\pi^2\hbar^3 c_s^2}\int_0^\infty dx\frac{x^4 e^x}{\left(e^x - 1\right)^2} = \frac{\pi^2 k^4 T^3}{10\hbar^3 c_s^2}, \tag{52}$$

where the integral on the left is $4\pi^4/15$. Now, from equation (46) for the heat ballistic flux we have

$$\left[I_Q\right]_{bl} = \frac{\pi^2 k^4 T^3}{10\hbar^3 c_s^2}\Delta T, \tag{53}$$

where $\Delta T = T_1 - T_2$, and since $T^3\Delta T = \Delta\,(T^4/4)$, finally

$$\left[I_Q\right]_{bl} = \frac{\pi^2 k^4}{40\hbar^3 c_s^2}\left(T_1^4 - T_2^4\right). \tag{54}$$

The similar result for photons is known as the Stefan – Boltzmann law differing from the phonon ballistic flux (54) by the factor of 2/3, as in the case of photons the number of allowed polarization is two.

Now let us get back to the diffusion transport of phonons.

**Thermal conductivity**

Phonon thermal conductivity is determined by (47) and is connected in the usual way with its specific value

$$G_k = \frac{\kappa A}{L + \lambda}, \tag{55}$$

so that finally the specific phonon thermal conductivity

$$\kappa = \frac{k^2 T}{h} \int_0^{+\infty} dx \left( \frac{M\lambda}{A} \right)_{ph} \frac{x^2 e^x}{\left( e^x - 1 \right)^2} \tag{56}$$

similar to the specific electron conduction [14]

$$\sigma = \frac{q^2}{h} \int_{-\infty}^{+\infty} dx \left( \frac{M\lambda}{A} \right)_{el} \frac{e^x}{\left( e^x + 1 \right)^2}. \tag{57}$$

Broadening function in the electron transport coefficients (eqn (84) in [1])

$$F_T(x) \equiv \frac{e^x}{\left( e^x + 1 \right)^2} \tag{58}$$

differs from the similar function in the phonon transport coefficients

$$F_T^{ph}(x) \equiv \frac{3}{\pi^2} \frac{x^2 e^x}{\left( e^x - 1 \right)^2}, \tag{59}$$

however, there is the similarity between them as shown on Fig. 2 of [1]. So, at least qualitatively, the electrical conductivity and thermal conductivity can be described similarly.

Thus, if the specific electrical conductivity for 3*D*-conductor is given by eqn (68) of [14]

$$\sigma = \frac{q^2}{h} \left( \frac{M\lambda}{A} \right), \tag{60}$$

where the coefficient $q^2/h \approx 38$ μS is the inverse value of the fundamental Klitzing constant (eqn (106) in [14]), then the specific thermal conductivity is given by

$$\kappa_{ph} = \frac{\pi^2}{3} \frac{k^2 T}{h} \left( \frac{M\lambda}{A} \right)_{ph}, \tag{61}$$

where the coefficient $(\pi^2/3)(k^2T/h) \approx 325$ pW/K with the factor $\pi^2/3$, opposite to that value, which is necessary to normalize the broadening function for phonons, and the number of modes per unit cross-sectional area of the conductor $M/A$ and the mean-free-pass $\lambda$ are estimated in the frequency gap $h\omega$, equal to approximately a few $kT$. The polarization $g$-factor $g = 3$ is assumed be included in the value of the number of modes $M$.

For thermoelectrics with the Seebeck coefficient $S \sim 2(k/q)$ and the dominanting phonon component of the specific thermal conductivity (61) for the $ZT$ product we can write

$$ZT \approx 4\frac{k^2T}{q^2}\frac{\sigma}{k+k_{ph}} \approx 4\frac{k^2T}{q^2}\frac{\sigma}{k_{ph}} \tag{62}$$

or either way, using (60) and (61),

$$ZT \approx \frac{M\lambda / A}{\left(M\lambda / A\right)_{ph}}, \tag{63}$$

where factor $12/\pi^2 \sim 1$ was omitted. This useful expression testifies that once thermoelectric is optimized with respect to Seebeck coefficient $S$ the corresponding $ZT$ product approximately shows the ratio of $M\lambda/A$ for electrons and phonons.

## Conclusions

In an effort to increase the Seebeck coefficient S we thus lower the ratio $M/A$ for electrons. On the other hand, the ratio of $M/A$ for the phonons are often much more, namely, $\sim 1$ nm$^{-2}$, so that their ratio in eqn (63) is about $\sim 0.1$ or even less. However, the electron mean-free-path is longer, thus in the best thermoelectrics $ZT \sim 1$. It now appears that the most promising way to improve $ZT$ is to suppress the mean-free-path of the phonons, without affecting the behavior of electrons (so called PGEC / Phonon-Glass-Electron Crystals [33, 34]).

For a long time we can not go beyond the $ZT \sim 1 – 3$. Experts argue that thermoelectrics with $ZT \sim 4 – 10$ would provide substantial progress in solving practical problems. Perspectives opened with the graphene research are briefly discussed in [35]. Hopes are still placed for nanostructured materials. Only experimental investigations will show is this perspective or not.

## References

1. Yu.A. Kruglyak. Electric current, thermocurrent, and heat flux in nano- and microelectronics: transport model // J. Thermoelectricity, N 6, p. 7 – 25, (2014).
2. Yu.A. Kruglyak Electric current, thermocurrent, and heat flux in nano- and microelectronics: selected topics // J. Thermoelectricity, N 6, p. 26 – 41, (2014).
3. R. Landauer, *IBM J. Res. Dev*. **1**, 223 (1957).

4. S. Datta, *Lessons from Nanoelectronics: A New Perspective on Transport* (World Scientific, Singapore, 2012).
5. M. Lundstrom, J. Changwook, *Near-Equilibrium Transport: Fundamentals and Applications* (World Scientific, Singapore, 2013).
6. T.S. Fisher, *Thermal Energy at the Nanoscale* (World Scientific, Singapore, 2013).
7. Yuriy Kruglyak, *J. Nanoscience*, Vol. 2014, Art. ID 725420, 15 pp. (2014); DOI: 10.1155/2014/725420.
8. J.M. Ziman, *Principles of the Theory of Solids* (Cambridge Univercity Press, Cambridge, 1964).
9. C. Kittel, *Introduction to Solid State Physics* (John Wiley and Sons, New York, 1971).
10. N.W. Ashcroft, N.D. Mermin, *Solid State Physics* (Saunders College, Philadelphia, 1976).
11. L.I. Anatychuk, *Thermoelectricity. V. 1. Physics of Thermoelectricity* (Bookrek, Chernivtsi, 2009).
12. Network of Computational Nanotechnology: www.nanohub.org.
13. S. Datta, *Fundamentals of Nanoelectronics – Basic Concepts*: www.nanohub.org/courses/FoN1.
14. Yu.O. Kruglyak, N.Yu. Kruglyak, M.V. Strikha, *Sensor Electronics Microsys. Techn*. **9**: N 4, 5 (2012).
15. Yu.A. Kruglyak, P.A. Kondratenko, Yu.M. Lopatkin, *J. Nano- Electron. Phys*. **5**: N 1, 01023 (2013).
16. Yu.A. Kruglyak, *Physics in Higher Education*, **19**: N 3, 99 (2013).
17. Yu.A. Kruglyak, N.E. Kruglyak, *Visnyk Odessa State Environ. Univ*. N 15, 213 (2013).
18. Yu.O. Kruglyak, M.V. Strikha, *Sensor Electronics Microsys. Techn*. **11**: N 1, 5 – 27 (2014).
19. K. Baheti, J.A. Malen, P. Doak *et al, Nano Lett.* 8, 715 (2008).
20. J. Balachandran, P. Reddy, B.D. Dunietz *et al, J. Phys. Chem. Lett.* **4**, 3825 (2013).
21. Y. Kim, W. Jeong, K. Kim *et al, Nature Nanotech*. **9**, 881 (2014).
22. Yu.A. Kruglyak. *ScienceRise*, **1**, N 2(6), 69 (2015).
23. Yu.A. Kruglyak. *ScienceRise*, **1**, N 2(6), 78 (2015).
24. L.I. Anatychuk, *Thermoelements and thermoelectric devices* (Naukova Dumka, Kiev, 1979).
25. F.W. Sears, G.L. Salinger, *Thermodynamics, Kinetic Theory, and Statistical Thermodynamics* (Addison-Wesley, Boston, 1975).
26. R. Kubo, *J. Phys. Soc. Japan*, **12**, 570 (1957).
27. L. Onsager, *Phys. Rev*. **37**, 405 (1931).
28. J.M. Ziman, *Electrons and Phonons. The Theory of Transport Phenomena in Solids* (Clarendon Press, Oxford, 1960).
29. P.E. Hopkins, J.C. Duda, P.M. Norris, *J. Heat Transfer*, **133**, 062401/1 – 11 (2011).
30. G. Chen, *Phys. Rev. B*, **57**, 14958 (1998).
31. H.-Y. Chiu, V.V Deshpande, H.W. Postma *et al*, *Phys. Rev. Lett*. **95**, 226101 (2005).

32. N. Zuckerman, J.R. Lukes, *Proc. ASME-JSME Thermal Eng. Summer Heat Transfer Conf.* N 32674 (Vancouver, Canada, 2007).
33. G.S. Nolas, D.T. Morelli, T.M. Tritt, *Ann. Rev. Mater. Sci*. **29**, 89 (1999).
34. Min Gao, D.M. Rowe, *J. Mater. Sci. Lett*. **18**, 1305 (1999).
35. Yu.O. Kruglyak, N.Yu. Kruglyak, M.V. Strikha, *Sensor Electronics Microsys. Techn*. **10**: N 4, 6 (2013).

Submitted 25.09.2015

*P.V. Gorskiy*

**P.V. Gorskiy**

Institute of Thermoelectricity of the NAS and MES of Ukraine,
1, Nauky Str., Chernivtsi, 58029, Ukraine

# OPTIMIZATION OF MATERIALS BASED ON *Bi-Te* POWDERS FOR THERMOELECTRIC ENEGY CONVERTERS

*Proceeding from the temperature and concentration dependences of the kinetic coefficients of thermoelectric material (TEM), the concentration dependences of thermoelectric figure of merit of powder based TEM were determined under the conditions of miniaturization for thermoelectric cooling and generation modes with different mean radii of powder particles. In so doing, the microscopic parameters of TEM necessary for taking into account the impact of size effects were directly determined on the basis of approximation models of their kinetic coefficients. The impact of size effects on the electrical conductivity of TEM was taken into account in the approximation of constant with respect to energy mean free path of charge carriers, and their impact on the lattice thermal conductivity – with regard to frequency dependence of the relaxation time of phonons scattered on each other due to anharmonicity of lattice thermal vibrations. In the latter case, both Umklapp and normal processes were considered capable of modifying scattering of electrons at layer boundaries It was shown that with the use of TEM powder with the mean particle radius 50 μm a gain in the figure of merit as compared to single crystal does not exceed 2 – 11 %. For smaller particle radii a gain can be greater. In particular, with the use of submicron TEM powders with the mean particle radius 0.1 μm the maximum thermoelectric figure of merit is increased by a factor of 1.18 – 2.15 as compared to single crystal. In so doing, the use of TEM powders with the mean particle radius 50 μm and more scarcely affects the optimal concentration of doping single-charge impurities, whereas transition to smaller mean radii of powder particles reduces it. For instance, with the mean particle radius 0.1μm it is reduced by a factor of 1.04 – 1.57 as compared to single crystal.*

**Key words:** electrical conductivity, thermoEMF, thermal conductivity, phonons, charge carriers, relaxation time, normal processes, Umklapp processes, mean free path, thermoelectric figure of merit.

## Introduction

Enhancement of the figure of merit of thermoelectric materials and thus, improvement of the output parameters and characteristics of thermoelectric energy converters with a simultaneous simplification and cheapening of their manufacturing process is one of the relevant tasks of up-to-date functional electronics. Theoretical and experimental investigations of powder based

thermoelectric materials pursued by various authors [1 – 5] give certain grounds to believe that the use of powders with the proper selection of the mean radius of their component particles will not only yield purely technological advantages in the manufacture of thermoelectric modules, but also improve their qualitative characteristics as compared to those of modules based on bulk single crystals.

It is common knowledge that the figure of merit of TEM depends on the concentration of charge carriers, hence, of doping impurities [6]. Moreover, for each temperature there exists such optimal charge carrier concentration whereby the figure of merit is maximal. However, when passing from single crystals to powder based materials, the effects related to charge carrier and phonon scattering at powder particle boundaries become apparent. In so doing, the kinetic coefficients of TEM are changed, hence, the maximum figure of merit and the corresponding optimal concentration of charge carriers can vary. Therefore, the purpose of this paper is optimization of powder based TEM for charge carrier concentration under the conditions of the impact of mean radius of particles constituting this material on its kinetic coefficients.

## Method of estimation of the figure of merit of powder based TEM versus mean particle radius and charge carrier concentration

Taking into consideration that powder boundary scattering has no impact on thermoEMF, and electron thermal conductivity and electrical conductivity in case of energy independence of electron mean free path depend on mean radius of powder particles through the same multiplier [7, 8], one can readily derive the following expression for thermoelectric figure of merit $Z$ of thin layer with respect to single crystal $Z_{mono}$:

$$Z/Z_{mono} = \frac{1+\kappa_{n,p(mono)}/\kappa_{l(mono)}}{Z_a^{-1}+\kappa_{n,p(mono)}/\kappa_{l(mono)}}. \qquad (1)$$

In this formula

$$Z_a = \left[\int_0^1\int_{-1}^1 y^2 \frac{k^*_{n,p}\sqrt{y^2-2zy+1}}{k^*_{n,p}\sqrt{y^2-2zy+1}+1}dzdy\right]\left[\int_0^1\int_0^1\int_{-1}^1 \frac{x^4\exp(x/\theta)y^2}{[\exp(x/\theta)-1]^2}\times\right.$$
$$\left.\times\left(\frac{k^*_{\|}\sqrt{y^2-2zy+1}}{1+k^*_{\|}Q_{l\|}(x)\sqrt{y^2-2zy+1}}+\frac{2k^*_{\|}\sqrt{y^2-2zy+1}}{1+k^*_{\|}Q_{l\|}(x)\sqrt{y^2-2zy+1}}\right)dzdydx\right]^{-1}\times \qquad (2)$$
$$\times\left\{\int_0^1 \frac{x^4\exp(x/\theta)}{[\exp(x/\theta)-1]^2}\left(\frac{1}{Q_{l\|}(x)}+\frac{2}{Q_{t\|}(x)}\right)dx\right\}.$$

In formulae (1 – 2), the following notations are introduced: $\kappa_{n,p(mono)}$ – electron or hole components of full thermal conductivity of single crystal, $\kappa_{l(mono)}$ – its lattice component, $k_{n,p}=r_0/l_{n,p}$ $r_0$ – mean radius of powder particles, $l_{n,p}$ – mean free path of electrons (holes) in single crystal, $k^*_{\|}=\left(r_0\gamma^2\theta/\rho\right)\left(k_BT_D/\hbar v_{\|}\right)^4\left(k_BT_D/\rho v^2_{\|}\right)$, $\theta=T/T_D$, $T$ – absolute temperature, $T_D$ – the

Debye temperature of material, $\gamma$, $\rho$ and $v_{||}$ – the Gruneisen parameter, the density and velocity of sound in TEM, respectively, $k_B$ – the Boltzmann constant, the rest of notations are commonly accepted. Index "||" means that the corresponding parameter is taken in a direction parallel to layer plane of TEM. Frequency polynomials $Q_{l||}(x)$ and $Q_{t||}(x)$, accordingly, are given below:

$$Q_{l||}(x) = x^4 + \mu x\,, \tag{3}$$

$$Q_{t||}(x) = \left(\mu + 3.125\theta^3\right)x\,. \tag{4}$$

Formulae (3) and (4) take into account both normal and Umklapp processes for the longitudinal (*l*) and transverse (*t*) phonon modes. Component $\mu x$ is responsible for Umklapp processes. It is also taken into account that phonon scattering due to normal processes takes place differently for the longitudinal and transverse modes, which is adequately described by other components in (3) and (4).

Relation (2) with regard to (3) and (4) was derived with the use of approaches developed in [7, 8] for the cases of spherical particles and contacts between them.

Thus, from relations (1 – 4) we see that for the calculation of thermoelectric figure of merit and efficiency of powder based TEM one must, using the experimental data, previously divide full thermal conductivity of single crystal into a component caused by electrons (holes) and lattice thermal conductivity. Also, based on the experimental data of the dependences of electrical conductivity, thermoEMF and thermal conductivity of single crystal on the temperature and charge carrier concentration, it is necessary to determine the temperature and concentration dependences of mean free path of electrons (holes) $l_{n,p}$ and parameter $\mu$ which is responsible for phonon scattering and, hence, for the value of TEM lattice thermal conductivity.

## Determination of the microscopic parameters of TEM based on the approximation of their kinetic coefficients

To determine the above microscopic parameters, the approximation models of experimental dependences of the kinetic coefficients of TEM are used that are built, for instance, by least-squares method [9]. On the basis of these models the microscopic parameters of TEM are determined as follows.

At first, on the assumption of energy independence of the mean free path of charge carriers, by the concentration and temperature-dependent thermoEMF from Eq. [10]

$$\alpha = \frac{k_B}{e}\left[\frac{2F_1(\eta)}{F_0(\eta)} - \eta\right] \tag{5}$$

the reduced chemical potential $\eta = \zeta / k_B T$ is determined. Following that, on the assumption of impurity conductivity, from the equation of constancy of the number of particles [10]

$$n_0 = \frac{4\left(2\pi m^*_{n,p} k_B T\right)^{3/2}}{\sqrt{\pi} h^3} F_{1/2}(\eta) \tag{6}$$

by the known density-of-state mass of electrons (holes) $m^*_{n,p}$, for instance, at temperature 300 K, charge carrier concentration $n_0$ is determined. Then, at each fixed concentration $n_0$ the temperature dependence of density-of-state effective mass $m^*_{n,p}$ is found. There is another method which is realized with the availability of data on charge carrier mobility. At first, charge carrier concentration is determined by the conductivity and mobility, and then from Eq. (6) – the density-of-state effective mass.

Following that, by the experimental temperature and concentration dependences of the electrical conductivity the mean free path of electrons (holes) $l_{n,p}$ on the temperature and charge carrier concentration is determined. For this purpose we employ the relation for the case of energy-independent mean free path of electrons (holes) [4]:

$$\sigma_{mono} = \frac{4 n_0 e^2 l_{n,p} F_0(\eta)}{\sqrt{2 m^*_{e,h} k_B T} F_{1/2}(\eta)}. \tag{7}$$

In formulae (5) – (7), $F_r(\eta)$ – the Fermi integrals of corresponding indices determined by the relation:

$$F_r(\eta) = \int_0^\infty \frac{x^r dx}{\exp(x-\eta)+1}. \tag{8}$$

Concerning the use of relation (6) for the determination of carrier concentration it should be noted that density-of-state effective mass of electrons (holes) is a function of not only temperature, but also charge carrier concentration. However, in case of materials for coolers an argument of approximation models is not charge carrier concentration, but the electrical conductivity at 300 K. For this case a simplifying assumption that at 300 K the effective mass does not depend on charge carrier concentration was invoked.

With a knowledge of $\eta$, one can use the Wiedemann-Franz relation to determine crystal thermal conductivity component due to free charge carriers:

$$\kappa_{n,p(mono)} = L\sigma T. \tag{9}$$

In so doing, the Lorentz number is equal to:

$$L = \left(\frac{k_B}{e}\right)^2 \left[\frac{3F_2(\eta)}{F_0(\eta)} - \frac{4F_1^2(\eta)}{F_0^2(\eta)}\right]. \tag{10}$$

Knowing the thermal conductivity due to free carriers, as well as the experimental thermal conductivity of TEM described by the corresponding approximation model, one can readily determine its lattice component. Knowing the temperature and concentration dependence of the lattice component of the thermal conductivity of TEM, it is easy, using the method developed in

[8] with regard to relations given in [11], to determine coefficient μ of polynomials (3), (4) characterizing frequency dependence of phonon-phonon scattering probability.

## Results of optimization of materials for coolers

Calculation of dependences of the figure of merit of powder based materials on the concentration of charge carriers was performed for *n*-type materials $Bi_2Te_{2.7}Se_{0.3}$ + (0.09…0.03) % $CdCl_2$ and *p*-type materials $Bi_{0.5}Sb_{1.5}Te_3$ + 4 % *Te* which are used for cooling modules. We employed the averaged experimental dependences given in [6, 9] of the kinetic coefficients $\alpha_{mono}$, $\sigma_{mono}$, $\kappa_{mono}$ of these materials on the temperature and electrical conductivity values at 300 K, proportional to charge carrier concentration. The calculations used parameters of phonon spectra and density-of-state effective masses of electrons and holes given in [12]. The calculations were performed on the basis of relations (1) – (4) by computer methods in the Mathcad-14 environment.

The concentration dependences of the figure of merit *ZT* of powder based materials obtained for various temperatures and particle radii are given in Fig. 1 – 4.

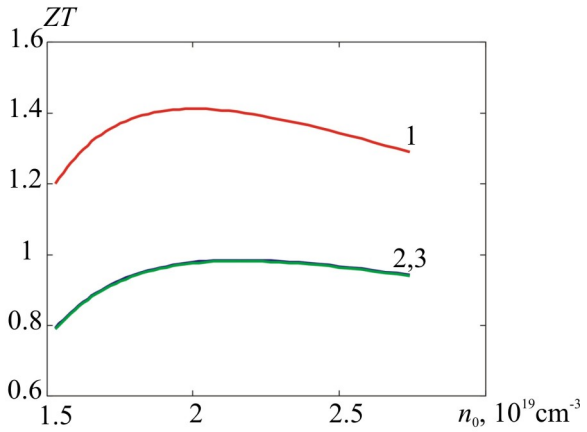


*Fig. 1. Concentration dependences of ZT of n-type TEM powders based on $Bi_2Te_{2.7}Se_{0.3}$ at temperature 300 K and mean particle radii, μm:1 – 0.1; 2 – 50; 3 – bulk crystal.*

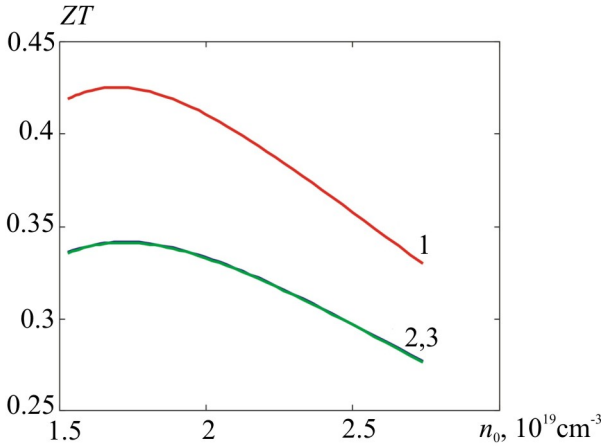


*Fig. 2. Concentration dependences of ZT of n-type TEM powders based on $Bi_2Te_{2.7}Se_{0.3}$ at temperature 150 K and mean particle radii, μm: 1 – 0.1; 2 – 50; 3 – bulk crystal.*

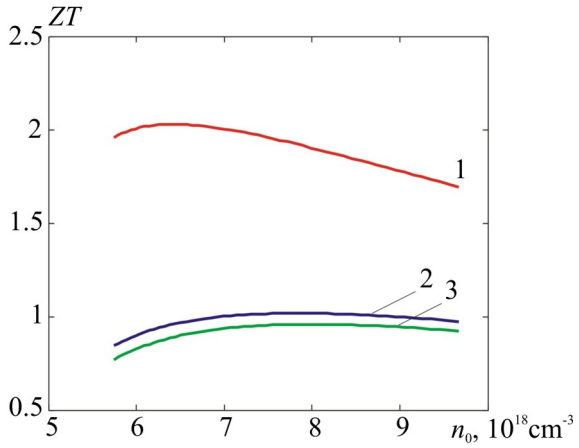


*Fig. 3. Concentration dependences of ZT of p-type TEM powders based on $Bi_{0.5}Sb_{1.5}Te_3$ at temperature 300 K and mean particle radii, μm: 1 – 0.1; 2 – 50; 3 – bulk crystal.*

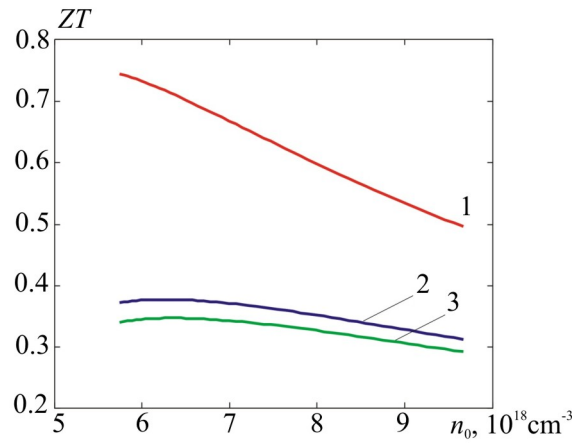


*Fig. 4. Concentration dependences of ZT of p-type TEM powders based on $Bi_{0.5}Sb_{1.5}Te_3$ at temperature 150 K and mean particle radii, μm: 1 – 0.1; 2 – 50; 3 – bulk crystal.*

From the figures it is seen that for the above materials at all temperatures when passing from single crystal to TEM powders there is a gain in the figure of merit. The figure of merit enhancement is attributable to the impact of size effects related to compatibility of charge carrier and phonon mean free paths to particle radius. In all cases there is radius-dependent optimal concentration of charge carriers whereby maximum thermoelectric figure of merit is achieved. However, as long as charge carrier and phonon mean free paths are measured by nanometers, there is no essential gain in the thermoelectric figure of merit when passing from single crystal to TEM powders with mean particle radii 50 μm and more. Essential gain, namely by a factor of 1.25 – 2.15 as compared to single crystal, is obtained with the use of TEM powders with the mean particle radius 0.1 μm. Nevertheless, the results imply that transition from a single crystal to TEM powders can be done without degrading the output parameters of coolers, and hence, one can achieve substantial simplification and cheapening of the process of manufacturing thermoelectric modules, including miniature-sized. More detailed information on the impact of mean radius of

TEM powder particles on the thermoelectric figure of merit and efficiency of materials for coolers is given in Table 1.

*Table 1*

*Predicted figures of merit of powder based materials for coolers*

| Mean particle radius, μm | Optimal concentration at 300 K | Conductivity at 300 K, S/cm | Thermoelectric figure of merit *ZT* at operating temperature | Gain as compared to single crystal, % |
|---|---|---|---|---|
| *n*-type cooling material at 300 K | | | | |
| 0.1 | $2 \cdot 10^{19}$ | 824 | 1.299 | 42 |
| 1 | $2.1 \cdot 10^{19}$ | 872 | 1.006 | 10 |
| 5 | $2.1 \cdot 10^{19}$ | 884 | 0.940 | 2.6 |
| 10 | $2.1 \cdot 10^{19}$ | 884 | 0.929 | 1.4 |
| 50 | $2.1 \cdot 10^{19}$ | 884 | 0.919 | 0.3 |
| Single crystal | | 884 | 0.916 | 0 |
| *n*-type cooling material at 150 K | | | | |
| 0.1 | $1.6 \cdot 10^{19}$ | 596 | 0.425 | 25 |
| 1 | $1.7 \cdot 10^{19}$ | 632 | 0.358 | 5 |
| 5 | $1.67 \cdot 10^{19}$ | 620 | 0.345 | 1.2 |
| 10 | $1.67 \cdot 10^{19}$ | 620 | 0.343 | 0.6 |
| 50 | $1.67 \cdot 10^{19}$ | 620 | 0.341 | 0 |
| Single crystal | $1.67 \cdot 10^{19}$ | 620 | 0.341 | 0 |
| *p*-type cooling material at 300 K | | | | |
| 0.1 | $6.31 \cdot 10^{18}$ | 744 | 2.031 | 111 |
| 1 | $6.92 \cdot 10^{18}$ | 840 | 1.508 | 57 |
| 5 | $7.30 \cdot 10^{18}$ | 900 | 1.224 | 27 |
| 10 | $7.38 \cdot 10^{18}$ | 912 | 1.138 | 18 |
| 50 | $7.81 \cdot 10^{18}$ | 972 | 1.085 | 11 |
| Single crystal | $7.89 \cdot 10^{18}$ | 984 | 0.961 | 0 |
| *p*-type cooling material at 150 K | | | | |
| 0.1 | $5.74 \cdot 10^{18}$ | 600 | 0.744 | 115 |
| 1 | $5.79 \cdot 10^{18}$ | 612 | 0.548 | 58 |
| 5 | $5.93 \cdot 10^{18}$ | 648 | 0.443 | 28 |
| 10 | $5.98 \cdot 10^{18}$ | 660 | 0.414 | 20 |
| 50 | $6.14 \cdot 10^{18}$ | 696 | 0.377 | 9 |
| Single crystal | $6.14 \cdot 10^{18}$ | 696 | 0.346 | 0 |

From the table, among other issues, it is seen that in the case of materials for coolers a transition from single crystal to TEM powders has little effect on the optimal concentration of charge carriers, and, hence, of *n*-type doping impurities, in *n*-type materials, and a much stronger effect – in *p*-type materials.

## Results of optimization of materials for generators

Calculation of dependences of the figure of merit of powder TEM on the concentration of charge carriers was performed for *n*-type materials $(Bi_2Te_3)_{0.9}(Sb_2Te_3)_{0.05}(Sb_2Se_3)_{0.05}$ and *p*-type materials $(Bi_2Te_3)_{0.25}(Sb_2Te_3)_{0.72}(Sb_2Se_3)_{0.03}$ which are used for generator modules. The averaged experimental dependences given in [9] of the kinetic coefficients $\alpha_{mono}$, $\sigma_{mono}$, $\kappa_{mono}$ of these materials on the temperature and electrical conductivity values at 300 K were employed. The calculations used parameters of phonon spectra and density-of-state effective masses of electrons and holes given in [10, 13].

The concentration dependences of the figure of merit *ZT* of powders of these materials obtained for various particle radii and temperatures are given in Fig. 5 – 8.

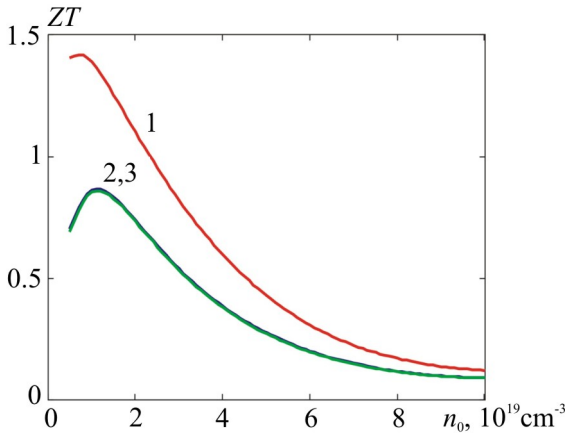


*Fig. 5. Concentration dependences of ZT of n-type TEM powder $(Bi_2Te_3)_{0.9}(Sb_2Te_3)_{0.05}(Sb_2Se_3)_{0.05}$ at temperature 300 K and mean particle radii, μm: 1 – 0.1; 2 – 50; 3 – bulk crystal.*

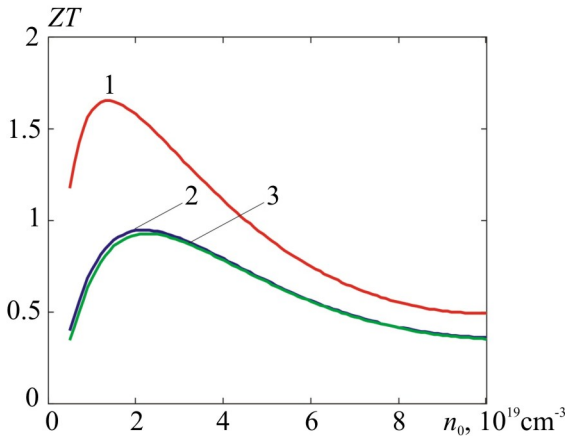


*Fig. 6. Concentration dependences of ZT of n-type TEM powder $(Bi_2Te_3)_{0.9}(Sb_2Te_3)_{0.05}(Sb_2Se_3)_{0.05}$ at temperature 450 K and mean particle radii, μm: 1 – 0.1; 2 – 50; 3 – bulk crystal.*

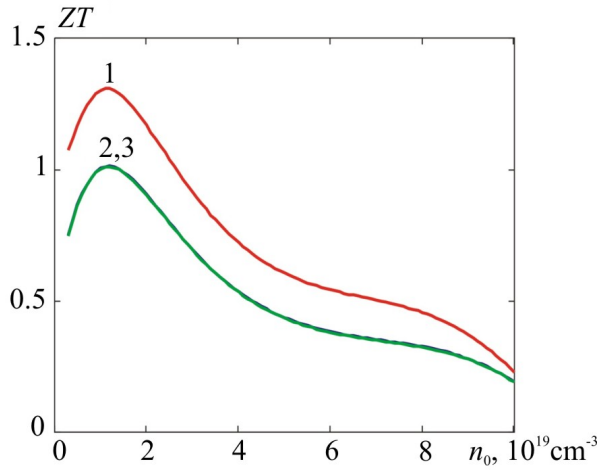


*Fig. 7. Concentration dependences of ZT of p-type TEM powder $(Bi_2Te_3)_{0.25}(Sb_2Te_3)_{0.72}(Sb_2Se_3)_{0.03}$ at temperature 300 K and mean particle radii, μm: 1 – 0.1; 2 – 50; 3 – bulk crystal.*

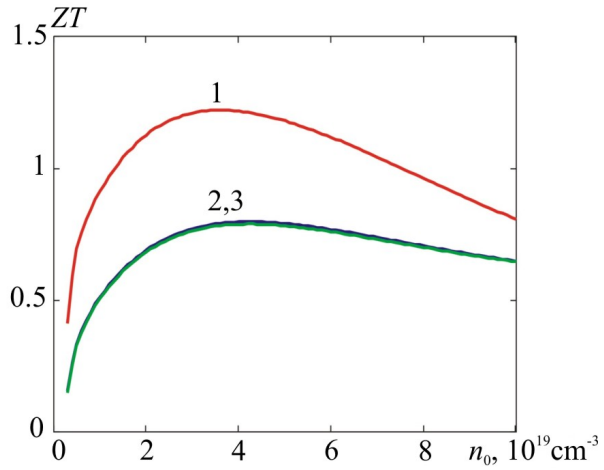


*Fig. 8. Concentration dependences of ZT of p-type TEM powder $(Bi_2Te_3)_{0.25}(Sb_2Te_3)_{0.72}(Sb_2Se_3)_{0.03}$ at temperature 450 K and mean particle radii, μm: 1 – 0.1; 2 – 50; 3 – bulk crystal.*

Just as in the case of materials for coolers, for each mean radius of powder particle there is optimal concentration of charge carriers whereby maximum thermoelectric figure of merit is achieved, and in the case of materials for generators it is expressed stronger than in the case of materials for coolers. Essential gain in the thermoelectric figure of merit, namely by a factor of 1.30 – 1.78 as compared to single crystal is obtained at mean particle radius 0.1 μm. More detailed information on the impact of mean radius of SPS-TEM particles on the thermoelectric figure of merit and efficiency of materials for coolers is given in Table 2.

From the table, among other issues, it is seen that with a decrease in the mean radius of TEM powder particles, the optimal concentration of charge carriers necessary for achieving maximum thermoelectric figure of merit is reduced. For instance, at the mean particle radius 0.1 μm it is reduced by a factor of 1.09 – 1.57 as compared to single crystal.

*Table 2*

*Predicted figures of merit of powder based materials for generators*

| Mean particle radius, μm | Optimal concentration at 300 K | Conductivity at 300 K, S/cm | Thermoelectric figure of merit *ZT* at operating temperature | Gain as compared to single crystal, % |
|---|---|---|---|---|
| *n*-type generator material at 300 K | | | | |
| 0.1 | $7.0 \cdot 10^{18}$ | 857 | 1.424 | 66 |
| 1 | $1.0 \cdot 10^{19}$ | 1128 | 1.011 | 18 |
| 5 | $1.1 \cdot 10^{19}$ | 1203 | 0.909 | 5.8 |
| 10 | $1.1 \cdot 10^{19}$ | 1203 | 0.887 | 3.3 |
| 50 | $1.1 \cdot 10^{19}$ | 1203 | 0.865 | 0.7 |
| Single crystal | $1.1 \cdot 10^{19}$ | 1203 | 0.859 | 0 |
| *n*-type generator material at 450 K | | | | |
| 0.1 | $1.4 \cdot 10^{19}$ | 1402 | 1.653 | 78 |
| 1 | $1.6 \cdot 10^{19}$ | 1517 | 1.243 | 34 |
| 5 | $1.9 \cdot 10^{19}$ | 1674 | 1.051 | 13 |
| 10 | $2.0 \cdot 10^{19}$ | 1723 | 1.003 | 8 |
| 50 | $2.2 \cdot 10^{19}$ | 1817 | 0.948 | 2 |
| Single crystal | $2.2 \cdot 10^{19}$ | 1817 | 0.928 | 0 |
| *p*-type generator material at 300 K | | | | |
| 0.1 | $1.1 \cdot 10^{19}$ | 704 | 1.308 | 30 |
| 1 | $1.2 \cdot 10^{19}$ | 743 | 1.083 | 7.2 |
| 5 | $1.2 \cdot 10^{19}$ | 743 | 1.024 | 1.4 |
| 10 | $1.2 \cdot 10^{19}$ | 743 | 1.019 | 0.9 |
| 50 | $1.2 \cdot 10^{19}$ | 743 | 1.011 | 0.1 |
| Single crystal | $1.2 \cdot 10^{19}$ | 743 | 1.010 | 0 |
| *p*-type generator material at 450 K | | | | |
| 0.1 | $3.5 \cdot 10^{19}$ | 1593 | 1.220 | 55 |
| 1 | $4.0 \cdot 10^{19}$ | 1758 | 0.956 | 21 |
| 5 | $4.0 \cdot 10^{19}$ | 1758 | 0.847 | 7.5 |
| 10 | $4.1 \cdot 10^{19}$ | 1790 | 0.824 | 4.6 |
| 50 | $4.1 \cdot 10^{19}$ | 1790 | 0.797 | 1.1 |
| Single crystal | $4.1 \cdot 10^{19}$ | 1790 | 0.788 | 0 |

## Comment on the role of phonon tunneling through vacuum gaps in thermo-electricity

Concerning the term used in the name of this section it should be noted that no phonon tunneling proper, i.e. acoustic vibration quanta through vacuum can exist, because classical experiment with a bell placed under the globe has not been refuted by anybody from classical or quantum standpoint. Then how should this term be understood? In Wikipedia, the free encyclopedia, one can come across a statement that it is a kind of "slang" which actually means tunneling of free charge carriers under the influence of their interaction with surface phonons in solids located on both sides of vacuum gap. However, this interpretation is inconsistent, because wave-particle nature of electrons (holes), and thus the possibility in principle of their passage through vacuum gap is unrelated to their interaction with phonons, either surface or bulk. It is more to the point to assert that this interaction under certain conditions can change in one direction or another possibility of passage of charge carriers through the gap. Nevertheless, the term "phonon tunneling" has a right to exist, if it is considered in the light of physical mechanism of heat transfer through vacuum gap between two piezoelectric, but not necessarily electrically conductive bodies. This mechanism was theoretically analyzed by the authors of [14] who, by the way, coined this term. The essence of this mechanism is as follows. Let there be two piezoelectric bodies 1 and 2, divided by vacuum gap. Lattice thermal vibrations in body 1 due to direct piezoelectric effect generate charge-density waves of alternating sign. Time- and space-varying charge, induced on the surface of body 1 adjacent to vacuum gap, generates in this gap an evanescent with the distance alternating electrical field, which, in turn, also induces time-and space-varying charge on the surface, hence, by induction, in the bulk of body 2. This charge, by virtue of inverse piezoelectric effect generates time- and space-variable deformations, i.e. vibrations, in the bulk of body 2. Thus, it turns out that phonons would "overflow" or "tunnel" through vacuum gap from body 1 to body 2. If these bodies are at different temperatures, such "overflow" is accompanied by heat transfer through vacuum gap which results in deviations from the Stephan-Boltzmann law. It is believed that if piezoelectric moduli of the bodies are rather great, the difference in temperatures is also great, and vacuum gap is small as compared to the wavelength of thermal phonon in a solid, then heat transfer through such gap can be great. This mechanism may act when one of the bodies is a piezoelectric (necessarily!), and another is a conductor, even metal. Then the field created in vacuum gap by the induced charge generates in the subsurface layer of conductor an alternating current. The latter, due to interaction of free charge carriers with phonons, leads to deformation, i.e. excitation of vibrations in the subsurface conductor layer, i.e. we again deal with a kind of "phonon tunneling". Apparently, exactly this variant of the above mechanism action generated its peculiar interpretation cited in Wikipedia. However, the author of this paper is not aware (at least among commonly used!) of such semiconductor thermoelectric materials which simultaneously would be strongly marked piezoelectrics. Therefore, there is no reason to be apprehensive about a drastic growth of thermal conductivity, hence of a drop in thermoelectric figure of merit and efficiency of powder based TEM due to an abnormally large

heat transfer through the pores. There is also no need in some radical revision of the existing theoretical concepts set forth, for instance, in [15] on the generalized conductivities and thermoEMF of nanostructured TEM, including spark plasma sintered SPS-TEM.

## Conclusions

1. The impact of phonon and charge carrier scattering at the boundaries of particles constituting SPS-TEM on the electrical conductivity and lattice thermal conductivity is the most essential factor which accounts for maintenance of thermoelectric figure of merit when passing from single crystal to SPS-TEM with the mean particle radius from 50 μm. Figure of merit improvement can be expected at smaller mean particle radii.
2. The use of powder based TEM instead of single crystals allows simplification and cheapening of the process of manufacturing thermoelectric modules without sacrificing their output parameters and characteristics.
3. A greater reduction of lattice thermal conductivity as compared to electrical conductivity creates conditions for improvement of the figure of merit of TEM when passing from the bulk single crystals to SPS-TEM.
4. The greatest gain in the figure of merit, namely a factor of 2.15 in the case of materials for coolers and by a factor of 1.78 for generator materials is achieved at particle radius 0.1 μm.
5. At particle radii exceeding 50 μm and temperatures 150 – 450 K the expected figure of merit improvement of considered materials with respect to corresponding single crystals does not exceed 11 % in the case of materials for coolers and 1.1 % in the case of generator materials.
6. There is no reason to be apprehensive about a drastic drop in the thermoelectric figure of merit and efficiency of SPS-TEM due to an abnormally large heat transfer through the pores.

## References

1. N.S.Lidorenko, V.A.Andriyako, L.D.Dudkin, and E.L.Nagayev, The Effect of Tunneling on the Efficiency of Thermoelectric Devices, *Doklady Akademii Nauk SSSR* 1295 (1969).
2. A.D.Terekhov, E.M.Sher, Structure of Dispersion and the Effective Values of Thermal Conductivity and Electric Conductivity Coefficients, in: *"Thermoelectric Materials and Films. Materials of All-Union Conference on the Deformation and Size Effects in Thermoelectric Materials and Films, Technology and Application of Films"* (Leningrad, 1976), p.211.
3. L.P.Bulat, I.A.Drabkin, V.V.Karatayev, V.B.Osvensky, and A.I.Sorokin, Effect of Scattering on the Boundaries on the Thermal Conductivity of Nanostructured Semiconductor Material $Bi_xSb_{2-x}Te_3$, *Physics of the Solid State* 52, 1712 – 1716 (2010).
4. S.Fan, J.Zhao, J.Guo, Q.Yan, J.Ma, and H.H.Hang, Influence of Nanoinclusions on Thermoelectric Properties of *n*-type $Bi_2Te_3$ Nanocomposites, *J. Electronic Materials* **40**(5), 1018 – 1023 (2011).

5. L.I.Anatychuk, P.V.Gorskiy, and V.P.Mikhalchenko, Impact of Size Effects on the Properties of Thermoelectric Materials, *J.Thermoelectricity* 1, 5 – 13 (2014).
6. L.I.Anatychuk, *Thermoelements and Thermoelectric Devices. Handbook* (Kyiv: Naukova Dumka, 1976), 726p.
7. P.V.Gorskiy, V.P.Mikhalchenko, Reduction of Thermoelectric Material Lattice Thermal Conductivity Using Shape-Forming Element Optimization, *J.Thermoelectricity* 1, 19 – 27 (2013).
8. P.V.Gorskiy, V.P.Mikhalchenko, On the Electric Conductivity of Contacting Particles of Thermoelectric Material, *J.Thermoelectricity* 2, 12 – 18 (2013).
9. L.I.Anatychuk, L.N.Vikhor, *Functionally Graded Thermoelectric Materials* (Institute of Thermoelectricity: Kyiv-Chernivtsi, 2012), 180p.
10. B.M.Goltsman, V.A.Kudinov, and I.A.Smirnov, *Semiconductor Thermoelectric Materials Based on $Bi_2Te_3$* (Moscow: Nauka, 1972), 320p.
11. P.G.Klemens, Lattice Thermal Conductivity, In: *Solid State Physics. Advances in Research and Applications, Vol.7, 1 – 98* (Academic Press. Inc. Publishers, New York, 1958), 526 p.
12. L.W.Da Silva, M.Kaviany, Micro-Thermoelectric Cooler: Interfacial Effect on Thermal and Electrical Transport, *Int. J. Heat and Mass Transfer* 478, 2417 – 2435 (2004).
13. *CRC Handbook of Thermoelectrics, edited by D.M.Rowe* (CRC Press, London, New York, 1995).
14. M.Prunilla, J.Meltaus, Acoustic Phonon Tunneling and Heat Transport due to Evanescent Electric Fields, *Phys. Rev. Let*. 105, 125501 (2010).
15. A.A.Snarskii, A.K.Sarychev, I.V.Bezsudnov, and A.N.Lagarkov, Thermoelectric Figure of Merit of Bulk Nanostructured Composites with Distributed Parameters, *Semiconductors* 46, 677 – 683 (2012).

Submitted 03.09.2015

**I.M. Rarenko[1], A.G. Shaiko-Shaikovsky[2], M.E. Belov[3]**

[1]Institute of Thermoelectricity of the NAS and MES of Ukraine, 1, Nauky str., Chernivtsi, 58029, Ukraine;
[2]Yu.Fedkovych Chernivtsi National University Chernivtsi, Ukraine, 58012, 2, Kotsyubinsky str;
[3]VAMP-AT Corporation, 99 Karmelyuk str., Chernivtsi, Ukraine

# PREDICTION OF THE VALUES OF NATURAL OSCILLATION FREQUENCIES IN THE DESIGN OF MULTI-STAGE STACKED THERMOELECTRIC STRUCTURES

*The paper deals with the possibility of theoretical determination during design phase of natural oscillation frequencies of thermoelectric coolers with different number of stages and different configuration. The natural oscillation frequencies were determined in parallel for products with regard to damping created by a number of structural members, as well as without regard to damping capacity of solder layers along thermoelement ends. Analysis and comparison of the obtained theoretical results was performed. The results of determination of natural oscillation frequencies of thermoelectric coolers (TEC) by using the system of Lagrange's equations of the second kind were compared with the calculated values obtained by the method of electrodynamic analogies.*

**Key words**: resonance, natural oscillation frequencies, damping.

## Formulation of the problem

For the purpose of cooling electronic products and radio equipment in order to assure their normal operating conditions, reduce their weight and dimensions, electronic devices and systems employ thermoelectric coolers (TEC) based on the well known Peltier principle. Depending on the purpose, specificity and parameters of electronic devices, their power and the amount of thermal energy released, TEC with different number of stages are used.

## Analysis of recent research

As is known, the operation of any type of carrier is characterized by certain frequency and amplitude of oscillations that are forced for the equipment installed thereupon. Provision of normal operation of TEC, their mechanical integrity is related to prevention of resonance effect on product exposure to certain frequencies of forced oscillations.

## Singling out parts of general problem unsolved before

Thus, to determine natural oscillation frequencies of products as early as during their design and development phase is an important engineering, technical and scientific problem.

For this purpose, apart from experimental methods, use is made of mathematical simulation which permits with assigned precision to calculate the required parameters (dimensions, shape of structural elements, corresponding materials) with the use of TEC models of different design and complexity [1]. For instance, the general view of a 3-stage TEC is represented in Fig. 1.

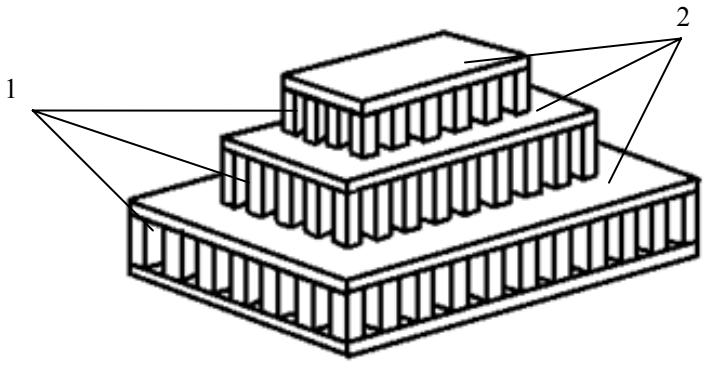


*Fig 1. General view of a 3-stage construction:*
*1 – thermoelements; 2 – heat spreaders.*

**Formulation of the goal of research.** The paper is concerned with a calculation of a 4-stage TEC structure the parameters of which are given below.

The number of thermoelements in each stage of devices studied in the paper was: $n_1 = 12$, $n_2 = 22$, $n_3 = 52$, $n_4 = 128$ (as an example, Fig. 1 shows a 3-stage cooler). The length of each thermoelement was $l = 1.4$ mm; cross-section: $0.7 \times 0.7$ mm. The thermoelements were made of bismuth telluride $Bi_2Te_3$ with the elasticity modulus $E = 6 \cdot 10^5$ kg/cm$^2$.

Heat spreaders 2 (Fig. 1) were made of glass ceramic plates 0.1 mm thick with copper current-conducting strips deposited thereupon. For attachment of thermoelements to current-conducting strip, solder was used on the lateral surface of heat spreaders with the thickness $\Delta = 1 \cdot 10^{-1}$ mm, the elasticity modulus was assumed to be $E_{II} = 1.2 \cdot 10^5$ kg/cm$^2$.

The masses of heat spreaders with the above number of thermoelements were: $m_1 = 10.92896 \cdot 10^{-5}$ kg; $m_2 = 4.55961 \cdot 10^{-5}$ kg; $m_3 = 1.95753 \cdot 10^{-5}$ kg; $m_4 = 1.31891 \cdot 10^{-5}$ kg. Such products, despite sufficiently small dimensions and mass, allow achieving temperature difference up to 20 °C on each stage, cooling essentially the electronic devices and products in operation. Mounting of TEC on mobile carriers (terrestrial, underwater, aeronautic, space) allows reducing considerably total weight of radioelectronic equipment and the dimensions of the entire installation.

## Formulation of the goal of research

The natural oscillation frequencies of stacked-type TEC were determined with the aid of developed mathematical model based on the use of differential Lagrange's equations of the second kind [2]:

$$\frac{d}{dt}\left(\frac{\partial T}{\partial \dot{x}_i}\right)-\frac{\partial T}{\partial x_i}=-\frac{\partial \Pi}{\partial x_i}-\frac{\partial \Phi}{\partial x_i}, \tag{1}$$

where: $T$ is kinetic energy of the system;

$\Pi$ is potential energy of the system;

$i$ is generalized coordinate;

$x_i$ is motion of $i$-th stage, $i$ = 1, 2, 3, 4;

$\Phi$ is dissipative function,

$t$ is time.

Kinetic energy of the system:

$$T=\sum_{i=1}^{4} T_i . \tag{2}$$

Potential energy of the system:

$$\Pi=\sum_{i=1}^{4} \Pi_i . \tag{3}$$

Dissipative function is proportional to the velocity of motion of system masses:

$$\Phi=\sum_{i=1}^{4} \Phi_i , \tag{4}$$

$$\Phi_i=\frac{1}{2}\beta_i \dot{x}_i^2 , \tag{5}$$

where $\beta_i$ is damping coefficient.

The paper is concerned with the case when the structure is composed of four stages of thermoelements which can be schematically shown as follows (Fig. 2):

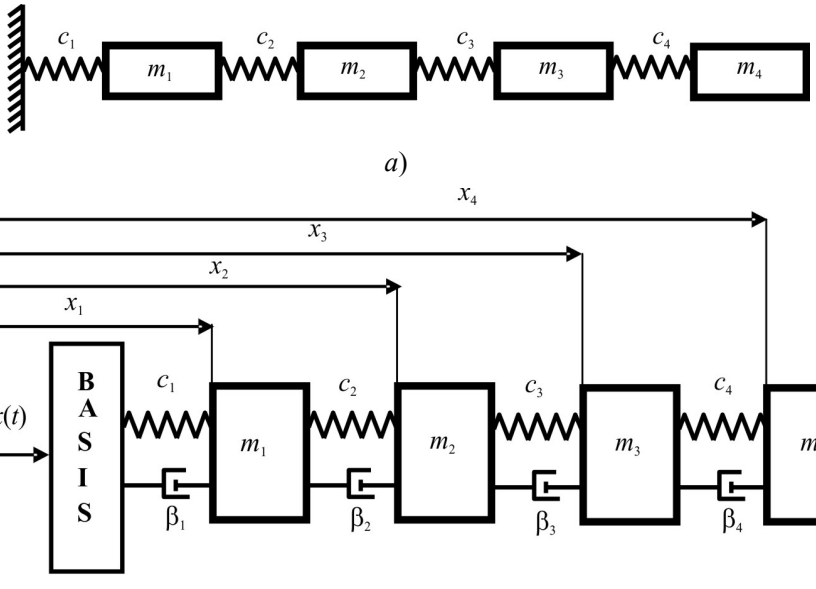


*Fig. 2. Design circuit of a 4-stage TEC; a) without regard to damping; b) with regard to damping.*

## The main results of the investigation

This paper is concerned with investigation of a specific 4-stage TEC, i.e. $i = 1, 2, 3, 4$. Here, $m_i$ is the masses of respective heat spreaders, and $c_i$ – the rigidity of thermoelements in each stage, respectively [1].

Solder layers along thermoelement ends have essentially lower values of elasticity modulus than the similar parameter of thermoelements material, i.e. they are characterized by a much lower rigidity. Therefore, it can be considered that solder layers along thermoelement ends in each stage serve as peculiar dampers reducing the values of product natural oscillations.

It is known that the dissipative function is nonlinear [4]. Account for this nonlinearity in complex technical systems is related to considerable, including mathematical, difficulties. Their account in many cases can introduce considerable specifications into the values of required parameter values with regard to products specificity and their operating conditions.

Due to small size of products under study, their dimensions and specificity of their use, it is assumed here that during the design phase of investigations the value of dissipative forces can be disregarded. (This assumption has been verified by calculation. The discrepancy in the results made 5 %).

The obtained results permit to foresee as early as during the design and development of future products possible cases of system resonance origination, take measures on "taking away" the values of natural oscillations from the values of resonance frequencies. It is particularly important in the development of responsible and expensive systems working on mobile carriers that have certain values of forced oscillations.

To verify the validity of calculated results, natural oscillation frequencies of the above TEC designs have been determined by independent approach, namely the method of electrodynamic analogies (EDA) known in theoretical mechanics.

For this purpose, the mechanical system under study is replaced by the respective electric analogies [3].

The electrical circuit of a 4-stage thermoelectric cooler will look as follows (Fig. 3):

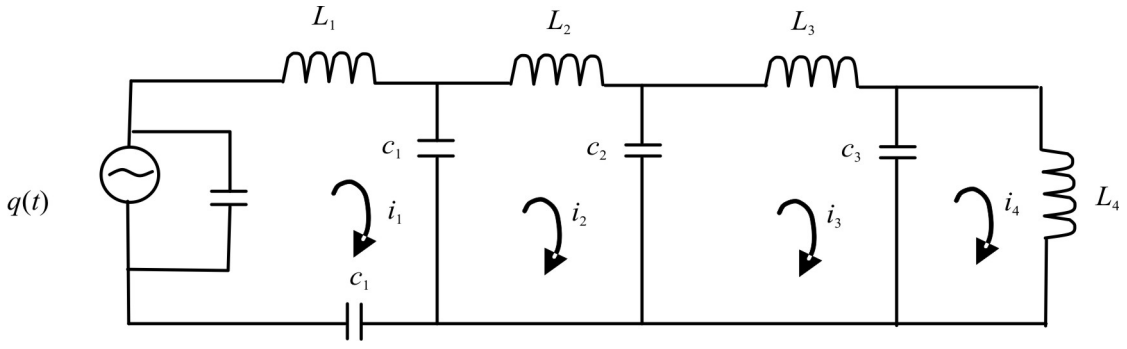


*Fig. 3. Electric schematic of a 4-stage TEC.*

The results obtained by using two independent design procedures for convenience of analysis and comparison are listed in Tables 1 – 4.

*Table 1*

*The values of natural oscillation frequencies of a 3-stage product (Hz) for $n_1 = 124$, $n_2 = 54$, $n_3 = 24$ with regard to damping*

| Number of thermoelements in a stage | 124 | 54 | 24 |
|---|---|---|---|
| Differential Lagrange's equations of the second kind | $2.177 \cdot 10^4$ | $4.027 \cdot 10^4$ | $5.50 \cdot 10^4$ |
| EDA | $2.22 \cdot 10^4$ | $4.234 \cdot 10^4$ | $5.76 \cdot 10^4$ |

*Table 2*

*The values of natural oscillation frequencies of a 3-stage product (Hz) for $n_1 = 124$, $n_2 = 54$, $n_3 = 24$ without regard to damping*

| Number of thermoelements in a stage | 124 | 54 | 24 |
|---|---|---|---|
| Differential Lagrange's equations of the second kind | $2.949 \cdot 10^6$ | $5.455 \cdot 10^6$ | $7.45 \cdot 10^6$ |
| EDA | $3.113 \cdot 10^6$ | $5.878 \cdot 10^6$ | $7.821 \cdot 10^6$ |

Analysis of the data in Tables 1 and 2 testifies that the spread in the values of natural frequencies is a function of the number of elements in a stage and varies within 1.94 % – 4.51 % (for products with regard to damping). At calculation without regard to damping this spread lies accordingly within 5.27 % – 5.19 %. With a reduction of the number of thermoelements in the stage, in both cases the spread in the obtained results is increased. Account of damping yields the values of natural frequencies, like in the previous cases, two orders lower, which is attributable to considerable effect of dampers on the values of natural vibration frequencies of the product. This makes it possible to "control" the values of natural vibration frequencies, varying them as required by the designer.

*Table 3*

*The values of natural oscillation frequencies (Hz) for a system with 4 degrees of freedom with regard to damping*

| Number of thermoelements in a stage | 124 | 54 | 24 | 12 |
|---|---|---|---|---|
| Differential Lagrange's equations of the second kind | $1.797 \cdot 10^4$ | $3.187 \cdot 10^4$ | $4.682 \cdot 10^4$ | $5.741 \cdot 10^4$ |
| EDA | $1.842 \cdot 10^4$ | $3.324 \cdot 10^4$ | $4.791 \cdot 10^4$ | $5.913 \cdot 10^4$ |

*Table 4*

*The values of natural oscillation frequencies (Hz) for a system with 4 degrees of freedom without regard to damping*

| Number of thermoelements in a stage | 124 | 54 | 24 | 12 |
|---|---|---|---|---|
| Differential Lagrange's equations of the second kind | $2.434 \cdot 10^6$ | $4.318 \cdot 10^6$ | $6.344 \cdot 10^6$ | $7.774 \cdot 10^6$ |
| EDA | $2.033 \cdot 10^6$ | $4.93616 \cdot 10^6$ | $6.872 \cdot 10^6$ | $8.234 \cdot 10^6$ |

Analysis of the data in Tables 2, 3 testifies that the spread in the values of natural oscillation frequencies obtained by two independent methods with regard to damping lies within 2.44 % –2.91 %, and on condition that damping is disregarded by calculation procedure, these values will be 6.49 % – 5.58 %.

## Conclusions

The results obtained by two independent methods showed the repeatability of 3 – 8 %, which confirms the quality and validity of mathematical models used in the paper.

Analysis and comparison of calculated results with the use of two independent procedures make it possible to estimate as early as during design phase possible values of natural oscillation frequencies of specific products used in practice, as well as those which are planned to be produced and used.

The elaborated algorithms and calculation programs on personal computers make it possible to determine natural oscillation frequencies of various TEC configurations and design, to estimate the advisability of using different embodiments of designed products, to determine the most acceptable variant for each type of equipment carrier. Permanent development and the advent of new structural materials used in electronics allows prompt selection during design phase of necessary material combinations for each specific device, assuring quality and functionality of equipment and complicated technical systems.

## References

1. A.V.Klepikovsky, E.N.Timofeeva, and A.G.Shaiko-Shaikovsky, Mathematical Model for Estimation of Factors Affecting the Values of Intrinsic Vibration Frequencies of Systems with Several Degrees of Freedom, *Proc. of International Symposium "Reliability and Quality 2009" (Penza, May 25 – 30, 2009),* Vol. 1, pp.300 – 302.
2. *Vibrations in Equipment, Handbook, Vol. 3. Vibrations of Machines, Constructions and Their Components,* Ed. by F.M.Dimentberg, K.S.Kolesnikov (Moscow: Mashinostroyenie, 1980), 544 p.
3. G.S.Pisarenko, V.V.Matveev, and A.N.Yakovlev**,** *Methods for Determination of Vibration Damping Characteristics of Elastic Systems* (Kyiv: Naukova Dumka, 1976), 86 p.
4. *Vibrations in Equipment, Handbook in 6 volumes, Vol. 6, Protection from Vibration and Shocks,* Ed. By K.V.Frolov (Moscow: Mashinostroeniye, 1981), 456 p.

Submitted 20.10.2015

**I.M. Rarenko[1], A.G. Shaiko-Shaikovsky[2], S.G. Dremlyuzhenko[1], M.E. Belov[3], A.I. Rarenko[1]**

[1]Institute of Thermoelectricity of the NAS and MES of Ukraine, 1, Nauky str., Chernivtsi, 58029, Ukraine;
[2]Yu.Fedkovych Chernivtsi National University
Chernivtsi, Ukraine, 58012, 2, Kotsyubinsky str.;
[3]VAMP-AT Corporation, 99 Karmelyuk str., Chernivtsi, Ukraine

# DEVICES FOR REMOTE TEMPERATURE MEASUREMENT OF VARIOUS OBJECTS BASED ON *CdSb* ANISOTROPIC THERMOELEMENTS

*The design, functioning principle, physical and technical parameters of the sensors of non-contact temperature measurement of various objects based on CdSb anisotropic thermoelements, are presented. The method of synthesis and growth of pure and structurally perfect CdSb single crystals to construct anisotropic thermoelements on them was developed.*

**Key words**: temperature measurement, sensors, anisotropic elements.

## Introduction

Many tracking systems, systems of measuring thermal signals and irradiance, technological and production processes, scientific studies and special equipment need and widely employ devices allowing signal measurement within the limits caused by a rather wide solid angle. This fact related to device design restricts considerably the equipment potential, complicates and elongates the research and measurement process, forces to supplement a design with rotary mechanisms for measuring unit, to install several such units in one system. The above mentioned requirements to design modification and complication reduce its precision and reliability, increase device dimensions and cost.

## Design of measuring unit for recording of energy signals with 180° solid angle of measurement

### Materials and methods

Numerous attempts are made to improve measuring systems, primarily increasing their precision and solid angle, enhancing the sensitivity and other device parameters.

In this work, the authors present a retrofit of a device for measurement of object irradiance, with the angle of coverage of measured signal increased to 180°.

Modernization of a device for irradiance measurement [1] led to expansion of viewing angle of thermal detector used in the device. Several design variants were considered with the

use of a flat thermopile of anisotropic thermoelements based on cadmium antimonide known and currently used for this purpose in thermal detectors [2]. For the experimental determination of viewing angle, a measuring bench was developed and assembled (Fig. 1) which is an optical bench accommodating a stabilized source of thermal radiation 2; radiation cutoff screen 7; blinds 4 and light guide 3 restricting the diameter of thermal radiation bundle; rotation table with angle meter 5 accommodating thermal detector holder and thermal radiation detector 6; as well as voltage stabilizer of thermal radiator 8, and recording device 9.

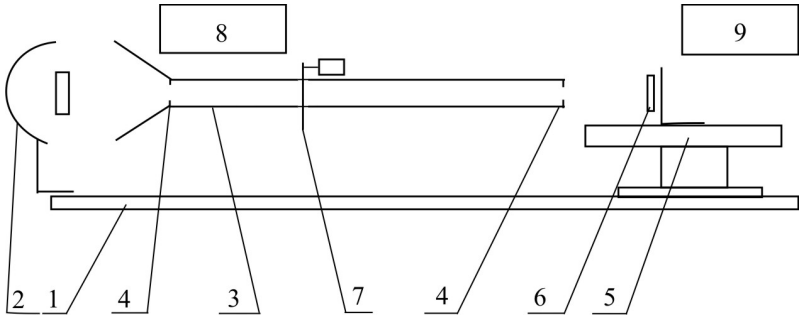


*Fig. 1. Measuring bench.*

The detector under test was placed into a holder in such a manner that the detector receiving pad was located on the optical axis of thermal bundle parallel to a beam. As a source of thermal radiation, an open nichrome spiral wound as a cone was used. The test was performed in natural heat exchange environment under normal conditions as follows. After switching and heating the installation for 2 min, the stable reading of detector recorder signal was recorded, which corresponded to background value of detector signal, then the shutter was opened for the time of exposition equal to 10 sec, the stable reading of detector recorder signal was recorded which corresponded to the measured heat flux value, following which the shutter was closed. The procedure was repeated seven times. Then the table with the thermal detector was rotated by the angle of 10° and a series of measurements was repeated for the newly set angle of receiving pad position with respect to incident heat flux. The results obtained were reduced to the average for each angular value and the respective indicatrix was built.

For further comparison and analysis the following thermal detector designs were considered for testing.

1. Nonselective thermal radiation detector [3] which is a flat thermopile of anisotropic thermoelements based on cadmium antimonide arranged in a package with a flat cover. The input window in the cover is restricted by a diaphragm located at the distance of 0.5 from the receiving pad.
2. Nonselective thermal radiation detector similar to the first one and characterized in that the cover in this case is shaped as a mirrored hemisphere. The input window is covered by IR filter of cadmium telluride single crystal, which assures the transmission region from 0.8 to 20 microns. The filter geometry corresponded to geometry of cosine head, and the receiving pad of thermal detector was located in a diametrical plane of mirrored hemisphere.

3. Nonselective thermal radiation detector similar to the first one and characterized in that the detector lacks IR filter and certain structural modifications have been introduced.

All thermal radiation detectors exposed to testing have volt-watt sensitivity at least 0.4 V/W. All the detectors have the identical size of receiving pad which is $6 \times 6$ mm$^2$. The geometrical dimensions of thermoelements and their number in all the cases were identical. Table 1 lists the values of output signal of a flat detector based on anisotropic thermoelements as a function of the intensity of heat flux incident on the receiving pad.

*Table 1*

*The values of flat detector output signal as a function of heat flux intensity*

| Heat flux intensity [W/mm $^2$] | 0.015 | 0.084 | 0.179 | 0.340 | 0.612 | 0.787 | 0.982 | 1.187 |
|---|---|---|---|---|---|---|---|---|
| Output signal [V] | 0.0026 | 0.0210 | 0.0646 | 0.1159 | 0.1802 | 0.2256 | 0.2118 | 0.3058 |

Fig. 2 shows the external view of one of the samples of detectors on anisotropic thermoelements for measuring heat flux intensity presented for testing.

*Fig. 2. External view of a detector based on anisotropic thermoelements (overall dimensions 16 × 16 mm).*

The results of comparative test are listed in Table 2. For convenience of analysis and comparison of characteristics, the measured data are represented in a normalized form (as a percentage ratio of electrical signal depending on the direction angle of thermal beam and maximum signal corresponding to a normal to receiving pad).

*Table 2*

*Results of measuring signal values as a function of measurement angle*

| Normalized value of detector electrical signal | | | | | | | | | | |
|---|---|---|---|---|---|---|---|---|---|---|
| Angle ° | 0 | 10 | 20 | 30 | 40 | 50 | 60 | 70 | 80 | 90 |
| Sample 1 | 0 | 0 | 0 | 1.2 | 6.6 | 19.2 | 41.4 | 68.9 | 94.8 | 100.0 |
| Sample 2 | 0.1 | 0.8 | 1.3 | 3.9 | 7.0 | 21.7 | 35.9 | 67.6 | 83.8 | 100.0 |
| Sample 3 | 2.7 | 12.2 | 24.0 | 37.2 | 48.7 | 64.5 | 78.1 | 88.1 | 96.8 | 100.0 |

The measuring head design developed and proposed by the authors has demonstrated high performance characteristics, the possibility of measurement in a wide coverage solid angle of 180°, which is not provided for by the first two detector designs. The design occupies very small space and its commercial version can be considerably reduced.

## Devices for distance temperature measurement of various objects based on *CdSb* anisotropic thermoelements

Heat flux sensors based on anisotropic thermoelements whose analogs were used to perform experimental studies of aperture angle, served the basis for creation of a variety of control and measuring instruments and systems of automatic regulation of technological processes. Examples of some of these devices are shown below.

Fig. 3 represents a measuring head of a specialized information-diagnostic complex for medical diagnostics which is based on the use of dynamic heat flow metering: noncontact remote observation of changes in thermal radiation within a certain period of time. Table 3 represents the main specifications of the elaborated measuring equipment.

*Fig. 3. Measuring head of a specialized information-diagnostic complex.*

*Table 3*

*Specifications of information-measuring equipment*

| № | Parameter | Measuring units | value |
|---|---|---|---|
| 1 | IR radiation detector, uncooled, based on anisotropic thermoelements, resolution, at least | V/W | 0.2 – 0.4 |
| 2 | Digital scale division value, at least | °C | 0.05 |
| 3 | Temperature of object under study | °C | 20 – 42 |
| 4 | Time of one exposure | sec | 1 |

*Table 3 (continued)*

| | | | |
|---|---|---|---|
| 5 | Time to reach the mode, not more | min | 30 |
| 6 | Time of continuous operation, not less | hour | 8 |
| 7 | Ambient temperature | °C | 10 – 35 |
| 8 | Relative air humidity at 25°C, not more | % | 80 |
| 9 | Work spectral domain | μm | 2 ÷ 16 |

The elaborated equipment and method of its use are intended for tooling backup of dynamic heat metering method. The equipment allows noncontact information reading from each point of object under study. With its aid, for instance, one can get information on the function disturbance of any organ even before the morphological changes take place, i.e. at the earliest stage.


*Fig. 4. Portable radiometer.*

Portable radiometer, Fig. 4, for temperature measurement on different coal mining plots. The radiometer is intended for measuring IR radiation energy density in the wavelength range of 1 ÷ 25 μm, for determination of temperature and temperature difference over a wide range:

– object temperature: -30 ÷ + 700°C;

– ambient temperature: from 5 to 60 °C;

– relative air humidity: not more than 90 %;

– atmospheric pressure: from 96 to 104 kPa (720 – 780 mm of mercury).

Accuracy of temperature difference measurement: at least ± 0.1°C.

*Table 4*

*Radiometer specifications*

| | | |
|---|---|---|
| 1 | Measurement range of thermal radiation density of objects. | 10 – 25000 W/m$^2$ |
| 2 | Limit of permissible basic relative error at ambient temperature deviation from fixed one within the operating temperature range | ± 0.1 % |
| 3 | Radiometer current consumption | Not more than 50 mA |
| 4 | Radiometer supply voltage | 9 V |
| 5 | Setting time: in discrete mode | 10 s |
| 6 | Setting time: in tracking mode | 1 s |
| 7 | Device weight | Not more than 0.6 kg |
| 8 | Overall dimensions | Not more than 190 × 90 × 50 mm$^3$ |

Use of device in coal mining industry allows determination of possible and real places of egress of carbon dioxide and gaseous hydrocarbons, places of geological heterogeneities in the mine face at penetrating, as well as localization of spontaneous fires in the mines.

*Fig. 5. General appearance of radiometer.*

Radiometer, Fig. 5, is intended for measurement of irradiance intensity in the wavelength range from 0.2 to 25 μm under normal climatic conditions:

– relative air humidity at 25 °C, not more than 80 %;

– atmospheric pressure, from 96 to 104 kPa (720 – 780 mm of mercury).

Filter supplied with the device provides for infrared (thermal radiation) transmission at the level of 62 % in the band of 0.8 ÷ 25 μm.

*Table 5*

*Radiometer specifications*

| | | |
|---|---|---|
| 1 | Irradiance measurement range | 10 ÷ 25000 W/m$^2$ |
| 2 | Limit of permissible basic relative error | Not more than ± 6 % |
| 3 | Limit of permissible basic relative error with the ambient temperature deviation from 20 °C, within the operating temperature range | ± 0.3 % |
| 4 | Radiometer supply current | Not more than 50 mA |
| 5 | Radiometer supply voltage | 9 V |
| 6 | Setting time | 1 s |
| 7 | Device weight | Not more than 0.6 kg |
| 8 | Overall dimensions, not more | 190 × 90 × 50 mm$^3$ |

Both the radiometer and devices based on this concept, can be used in engineering, medicine, agriculture and other fields to measure the density of thermal radiation flux from the heated objects; to measure heat losses in heat power engineering, machine building, construction industry, etc.

## Conclusion

1. The use of device in coal mining industry permits to determine methane egress in a mine face at penetrating, to localize spontaneous fires in coal mines.
2. To use the device as noncontact temperature controller in technological processes:
   – at quenching of technical glass for the temperature level of 600 ÷ 700 °C, to an accuracy at least ± 0.5;
   – at packing of pills and capsules in pharmacological industry at 90 ÷ 200 °C, to an accuracy at least ± 0.2.
3. In the instrumentation and test equipment as the sensors of automatic control systems in the chambers: of solar radiation, heat and cold, humidity with the resolution at least 8 g of water in 1 m$^3$, rain and dropping effect from individual drops to tropical shower.
4. In agriculture:
   – in cattle breeding;
   – in greenhouse business.
5. In meteorology:

– rain intensity sensor;
– actinometers.

6. In medicine:
   – for the noninvasive noncontact functional diagnostics of kidneys, thyroid glad, lungs and other diseases;
   – determination of placenta function, healing of postsurgical and traumatic stitches, etc.;
   – localization of inflammatory processes, etc.
7. In construction industry:
   – to detect the areas of largest real heat losses through external walls and to measure the value of these heat losses in watts from one square meter of surface;
   – for quality control of thermal insulation of heat pipelines and for measuring the value of heat losses from the unit surface of heat pipelines in watts from one square meter of surface;
   – for quality control of heat-insulating materials and structural elements by their real heat-insulating properties in units of heat flux density, i.e. $W \cdot m^{-2}$, etc.
8. Besides the ones listed above, other specific application fields are possible that are solved by using thermal phenomena associated with the process or function.

## References

1. I.M.Pilat, B.G.Shabashkevich, S.I.Pirozhenko, et al., Radiometers of Irradiance on the Anisotropic Thermoelements, Optical Journal 67(3), pp. 83 – 85 (2000).
2. Declarative patent for utility model, 25458 (Ukraine). Radiation Detector/ B.G.Shabashkevich, Yu.D.Dobrovolsky.-2007.-Bul. № 12.
3. Yu. D.Dobrovolsky, B.G.Shabashkevich, Anisotropic Thermal Radiation Detector Based on Cadmium Antimonide, Tekhnologiya i Konstruirovanie v Elektronnoi Apparature 1, 31 – 33 (2009).

Submitted 17.09.2015.

*R.R. Kobylianskyi*

**R.R. Kobylianskyi[1,2], I.A. Moskalyk[1]**

[1]Institute of Thermoelectricity of the NAS and MES of Ukraine, 1 Nauky str., Chernivtsi, 58029, Ukraine;
[2]Yu. Fedkovych Chernivtsi National University, 2, Kotsyubinsky str., Chernivtsi, 58012, Ukraine

*I.A. Moskalyk*

# ON TEMPERATURE DISTRIBUTION IN HUMAN HEAD AT GIVEN THERMAL FLUXES ON ITS SURFACE

*The paper presents a review and analysis of the existing physical and computer models of human head cooling. With the aid of object-oriented computer simulation of currently available physical models the distributions of temperature in human head at given thermal fluxes on its surface are determined. The disadvantages of the existing models of human head are determined and the ways for their improvement are proposed.*

**Key words:** thermoelectric cooling, human head cooling, brain hypoxia, computer simulation.

## Introduction

Brain oxygen starvation (hypoxia) is a relevant problem in medical practice which is due to inadequate oxygen flow to nervous tissues. This happens for two reasons: the lack of oxygen in blood or disturbance of blood delivery to brain. Hypoxia is observed at cerebrovascular accidents, shock states, acute cardiovascular insufficiency, atrioventricular heart block, head injuries and asphyxia of different origin. Brain hypoxia can be a complication of cardiac surgery and vascular procedures, as well as in the early postoperative period – at hypoxic brain edemas, intoxication and central nervous system injuries.

It is known that brain cooling reduces its oxygen requirement, increases resistance to hypoxia, thus increasing permissible duration of oxygen starvation. Thus, for instance, cooling by 5 °C extends brain lifetime several times [1 – 4].

For a correct design of brain hypothermia devices it is necessary to know the distributions of human brain temperature. However, physical models and the results of computer simulation of thermal processes in human head reported in the literature are contradictory.

In [5], a two-dimensional mathematical model was developed to study brain cooling of newborns and adults at cold water diving. The model of head is simplified and has the form of a hemisphere composed of brain, skull and skin. The results of simulation show that for newborns the temperature of blood in carotid artery is reduced by as low as 0.1 °C within 5 min at diving to water with temperature $T = 2$ °C, and no cooling was observed in this case for adults. In [6], a three-dimensional model of human head was built with regard to thermophysical properties of

human head constituent layers. Computer simulation of human head cooling with ice was performed. It is established that brain cooling will be observed only in the case when blood perfusion is disregarded. Brain cooling with the aid of cooling helmet of temperature $T = 0$ °C was studied, in which case there is slight cooling of brain cortex, while brain nucleus temperature remains constant ($T = 37$ °C). Besides, this paper studies cooling of blood that circulates through the neck. It is established that cooling of arterial blood will take place only in the case when blood rate will be reduced by an order of magnitude, which is impossible under real conditions. A three-dimensional (3D) simulation of human head was done in [7]. In this case a physical model comprises four layers: the white and grey substance, skin, and skull. It is established that slight temperature reduction of brain surface will take place, but similar to [6] the model does not take into account blood perfusion. In [8], computer simulation of brain cooling of newborns and adults with the aid of cooling helmet is performed using Comsol Multiphysics. The results for newborns show that only 5 – 6 mm of near-surface brain layer are cooled, and the temperature of brain nucleus is not reduced even after six hours of use. The results of simulation of adult head show that at a minimum temperature of cooling helmet $T = 0$ °C the temperature of brain is reduced by 0.4 °C. In [9], an experimental study of human head and neck cooling was performed on 5 volunteers at the ages from 31 to 48. Cooling was performed for 30 min with the aid of cooling helmet and collar made of a double nylon layer, with openings for air blasting in the inner layer, air temperature 14.5 °C, and flow rate 42.5 l/s. Brain temperature control was performed via MRT-scanner. It was established that brain temperature within 30 min was reduced by 0.45 °C, and the esophagus temperature – by 0.16 °C. The results obtained testify that there is a slight cooling of human brain and circulating blood.

Therefore, *the purpose of this paper* is to reveal the incorrectness of the existing models of human head and to determine the distributions of temperature in human head at given thermal fluxes on its surface.

## Physical model of human head

Physical model was created on the basis of the existing models of human head and is a hemisphere of radius $R$ equal to the average radius of an adult human head (Fig. 1). This hemisphere has near-surface layers 1 – 3 whose thicknesses are equal to the average thicknesses of scalp $h_1$, subcutis layer $h_2$ and cranial bones $h_3$, respectively. Inside the hemisphere there is brain 4 of radius $R_4$. The corresponding layers 1 – 4 are considered as volumetric sources of heat. In each of them uniformly in the volume of the layer a metabolic heat $q_{METi}$ ($i = 1..4$) is generated, and heat exchange with the circulating blood takes place which is assigned by blood perfusion coefficient $\omega_{bi}$. In so doing, brain is a biological tissue with high perfusion of blood, and blood temperature is constant ($T_b = 37$ °C). The temperatures at the boundaries of corresponding layers are $T_1$, $T_2$, $T_3$, $T_4$. The thermophysical properties of these biological layers are given in Table [10].

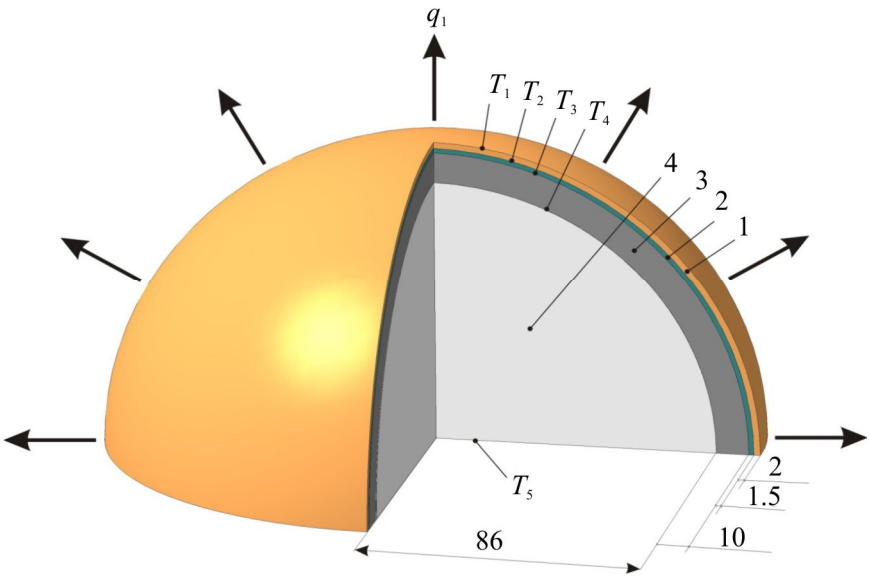


*Fig. 1. Physical model of human head.*

*Table*

*Thermophysical properties of human head biological layers [10]*

| Anatomical organization of human head | Thermal conductivity (k) (W/m·K) | Density (ρ) (kg/m$^3$) | Specific heat ($C_p$) (J/kg·K) | Perfusion ($W_b$) (l·s$^{-1}$ m$^{-3}$) | Metabolism ($q_{met}$) (W/m$^3$) |
|---|---|---|---|---|---|
| Scalp | 0.47 | 1000 | 3680 | 1.5 | 363 |
| Subcutis | 0.16 | 850 | 2300 | 0.2 | 130 |
| Scull | 1.16 | 1500 | 1591 | 0.15 | 130 |
| Brain | 0.49 | 1080 | 3850 | 8.5 | 10437 |
| Blood | 0.5 | 1069 | 3650 | – | – |

The upper surface of hemisphere is in the state of heat exchange with the environment (due to radiation and convection) or with the cooling helmet (with the assigned integral heat transfer coefficient). In so doing, $q_1$ is the density of thermal flux dissipated from human head to the environment. The temperature of the lower hemisphere surface is $T_5$ = 37 °C.

## Mathematical description of physical model

A general equation of heat exchange in biological tissue is as follows [1 – 10]:

$$\rho_i \cdot C_i \cdot \frac{\partial T}{\partial t} = \nabla(\kappa_i \cdot \nabla T) + \rho_b \cdot C_b \cdot \omega_{b_i} \cdot (T_b - T) + q_{met_i}, \quad (1)$$

where $i$=1..4 are corresponding layers of human head physical model,

$\rho_i$ is the density of corresponding biological tissue layer (kg/m$^3$),
$C_i$ is specific heat of corresponding biological tissue layer (J/kg·K),
$\rho_b$ is blood density (kg/m$^3$),
$C_b$ is specific heat of blood (J/kg·K),
$\omega_{bi}$ is blood perfusion rate in corresponding biological tissue layer ($m^3 \cdot s^{-1} \cdot m^{-3}$),
$T_b$ is human blood temperature (K),
$q_{meti}$ is the amount of metabolic heat of corresponding layer (W/m$^3$),
$T$ is absolute temperature (K),
$\kappa_i$ is thermal conductivity of biological tissue (W/m·K),
$t$ is time (s).

The summand on the left-hand side of equation (1) is the rate of change in thermal energy comprised in the unit volume of biological tissue. Three summands on the right-hand side of this equation are the rate of change in thermal energy due to thermal conductivity, blood perfusion and metabolic heat, respectively.

The equation of heat exchange in biological tissue (1) should be solved with the following boundary conditions (2) – (3):

$$\begin{cases} q_1 = q_{rad} + q_{conv} = \varepsilon \cdot \sigma \cdot (T^4 - T_0^4) + h_{conv} \cdot (T - T_0) \\ або \\ q_1 = h_{fluid} \cdot (T - T_{fluid}) \end{cases}, \quad (2)$$

$$T_5 = 310 \text{ K}, \quad (3)$$

where $q_1$ is the density of heat flux dissipated from human head to the environment, $q_{rad}$ is the density of heat flux due to radiation, $q_{conv}$ is the density of heat flux due to convection, $\varepsilon$ is emissivity factor, $\sigma$ is the Boltzmann constant, $T$ is absolute temperature, $T_0$ is ambient temperature, $h_{conv}$ is coefficient of convective heat exchange, $h_{fluid}$ is coefficient of convective heat exchange with fluid, $T_{fluid}$ is fluid temperature.

## Computer simulation results

In order to determine thermal influence on human head, a 3D computer model of a head whose surface is in contact with cooling helmet was created. To construct the model, Comsol Multiphysics software package was employed [11], allowing simulation of thermophysical processes in human body biological tissue with account of blood circulation and metabolism. Calculation of temperature and heat flux density distributions inside human head was done by finite element method (Fig. 2). [12].

Object-oriented computer simulation was employed to determine temperature distribution inside human head. As an example, Fig. 3 shows temperature distribution in the axial section of human head with the total thermal flux from its surface $Q$ = 10 W.

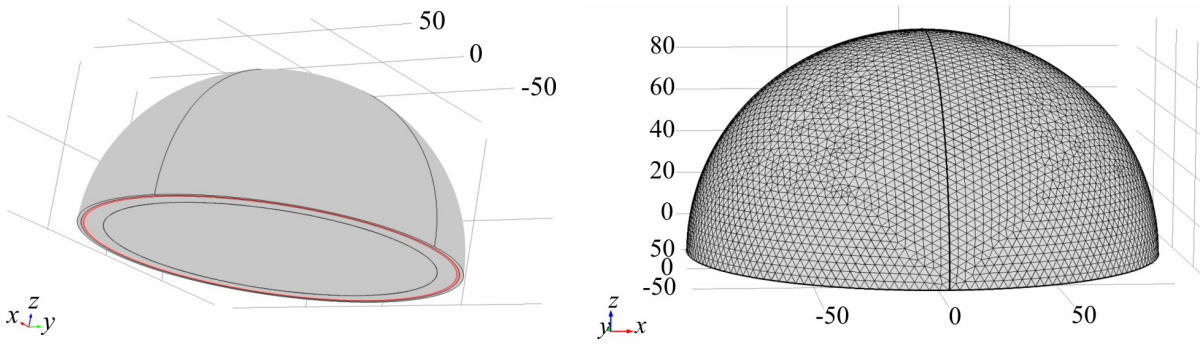


*Fig. 2. Finite element method mesh in COMSOL MULTIPHYSICS computer program.*

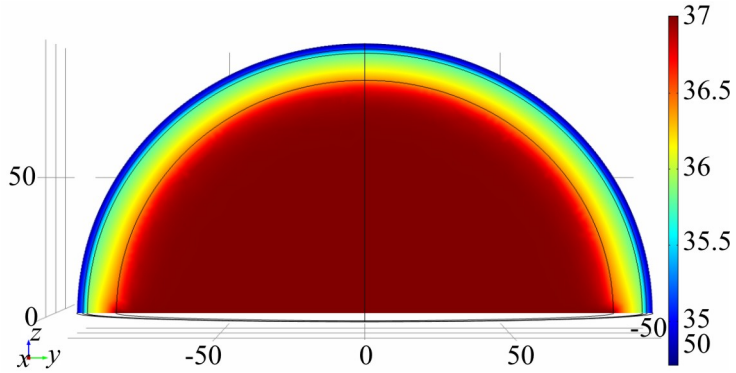


*Fig. 3. Temperature distribution in the axial cut of human head with the total thermal flux from its surface Q = 10 W.*

The range of values of thermal fluxes from the surface of human head is $Q = 10 \div 100$ W, which is limited by minimum allowable head surface temperature + 2 °C. For convenience of comparison of said thermal modes, Fig. 4 shows temperature distributions along the radius of head hemisphere with the respective values of thermal fluxes from human head surface.

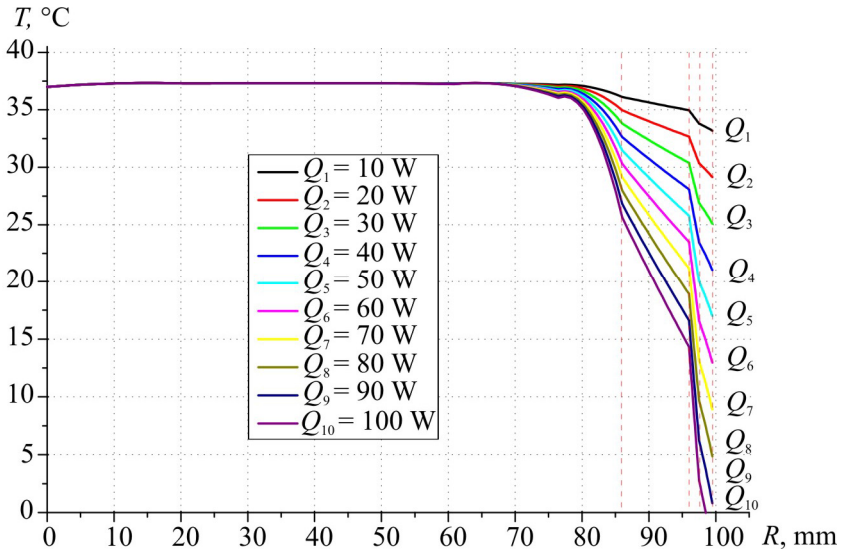


*Fig. 4. Effect of cooling power Q on temperature T distribution along radius R of human head hemisphere.*

From Fig. 4 it can be seen that on condition of maintenance of a minimum allowable temperature of head skin (+ 2 °C), only 3 mm of human brain surface layer can be cooled to the required temperature + 32 °C. In so doing, the temperature of brain nucleus remains constant (+ 37 °C). In this case, 90 W of heat is removed from the head, which according to the literature data [13] is 90 % of total heat production of human organism. However, in actual practice, brain must be cooled, since heat removal on the level of 90 W exceeds 6-fold the total heat production of human head. As a result, blood that passed through the head must be cooled, and passing through human body it must cool the entire human organism, and, on coming back to the head, the temperature of blood must be somewhat lower than + 37 °C which in the existing models is given by a constant. It is apparent that exactly this fact is the main disadvantage of the existing physical and computer models of human head.

Thus, currently available approaches to creation of physical models and computer simulation of human head assuming arterial blood temperature to be constant ($T_{blood}$ = + 37 °C), should be improved by taking into account gradual cooling of circulating blood and heat capacity of the entire human organism.

## Conclusions

1. With the aid of object-oriented computer simulation on the basis of the existing physical models the distributions of temperature in human head were determined under given thermal fluxes on its surface. It was established that on condition of maintenance of a minimum allowable temperature of head skin (+ 2 °C), only 3 mm of human brain surface layer can be cooled to the required temperature + 32 °C, while the temperature of brain nucleus remains constant (+ 37 °C).
2. It was established that currently available approaches to creation of physical models and computer simulation of human head assuming arterial blood temperature to be constant ($T_{blood}$ = + 37 °C), should be improved by taking into account gradual cooling of circulating blood and heat capacity of the entire human organism.

## References

1. Liu Jing, Cooling Strategies and Transport Theories for Brain Hypothermia Resuscitation, *Frontiers of Energy and Power Engineering in China* **1**(1), 32 – 57 (2007).
2. A.M.Belous, V.I.Grischenko, *Cryobiology* (Kyiv: Naukova Dumka, 1994), 431 p.
3. T.M.Darbinyan, A.N.Zirakadze, S.M.Zolnikov, P.Ya.Kintraya, B.A.Komarov, S.N.Kopshev, N.P.Kupin, and K.D.Chachava, *Artificial Hypothermia* (Moscow: Soviet Encyclopedia, 1989).
4. R.R.Kobylianskyi, I.A.Moskalyk, The Prospects of Using Thermoelectricity for Human Head Cryotherapy, *J.Thermoelectricity* 4, p. 85 – 94 (2015).
5. Xiaojiang Xu, Peter Tikuisis, and Gordon Giesbrecht, A Mathematical Model for Human

Brain Cooling during Cold-Water Near-Drowning, *J. Appl Physiol.* **86**, 265 – 272 (1999).

6. Brian H. Dennis, Robert C. Eberhart, George S. Dulikravich, and Steve W. Radons, Finite Element Simulation of Cooling of Realistic 3-d Human Head and Neck, *J. Biomechanical Engineering*, January (2004).
7. Matthew A. Neimark, Angelos-Aristeidis Konstas, Jae H. Choi, Andrew F. Laine, and John Pile-Spellman, Brain Cooling Maintenance with Cooling Cap Following Induction with Intracarotid Cold Saline Infusion: A Quantitative Model, *J.Theoretical Biology* **253**(2), 333 – 44 (2008).
8. Michael Christiansen, Nikolai Rakhilin, Anna Tarakanova, and Kevin Wong, *Modeling Brain Cooling Treatment Approved for Hypoxic-Ischemic Encephalopathy in Infants to Treat Stroke and Cardiac Arrest in Adult Patients*, Cornell University. Fall 2010.
9. B.A.Harris, P.J.D.Andrews, I.Marshal, T.M.Robinson, and G.D.Murray, Forced Convective Head Cooling Device Reduces Human Cross-Sctional Brain Temperature Measured by Magnetic Resonance: a Non-Randomized Healthy Volunteer Pilot Study, *British J.Anaesthesia* **100** (3), 365 – 72 (2008).
10. D.Fiala, K.J.Lomas, and M.A.Stohrer, Computer Model of Human Thermoregulation for a Wide Range of Environmental Conditions: the Passive System, *J. Appl. Physiol*. **87**(5): 1957 – 1972 (1985).
11. *COMSOL Multiphysics User's Guide*, COMSOLAB, 2010, 804 p.
12. A.D.Legostayev, *Finite Element Method, Synopsis* (Kyiv: KNUBA, 2004), 112 p.
13. S.C.Jiang, N.Ma, H.J.Li, and X.X.Zhang, Effects of Thermal Properties and Geometrical Dimensions on Skin Burn Injuries, *Burns* **28**, 713 – 117 (2002).

Submitted 28.10.2015

# NEWS
# OF INTERNATIONAL THERMOELECTRIC ACADEMY

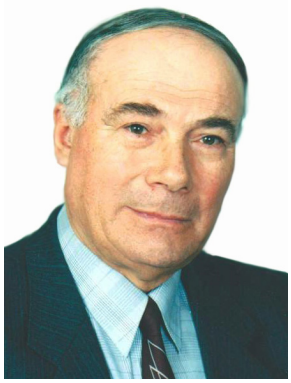

# CASIAN
# ANATOLIY IRRADIONOVICH

(Dedicated to 80th birthday)

In November 2015 Anatoliy Irradionovich Casian, a well-known scientist, Doctor of Science in Physics and Mathematics, professor, academician of the International Thermoelectric Academy celebrated his 80th birthday.

Anatoliy Irradionovich Casian was born on November 17, 1935 in the village of Kolikautsi, Brichany district, Moldova.

In 1957 he graduated with honours from Kishinev State University (now State University of Moldova) in the specialty "theoretical physics". In the same year he entered the post-graduate course at that university; in 1961 defended his PhD thesis, and in 1988 – doctoral thesis in Physics of Semiconductors. In 1990 A.I. Casian was awarded the title of professor.

During 1960 – 1969 he occupied different positions in the Academy of Sciences of Moldova. Up to 1976 he headed Theoretical Mechanics Faculty of Kishinev Polytechnic Institute. In 1976 – 1982 he worked in Moldova Branch of Institute of Current Sources of Moscow Scientific-Industrial Association "Kvant" in the position of leading researcher, and then – director of the branch.

From May 1982 till today he is professor of Theoretical Mechanics Faculty of Technical University of Moldova.

Anatoliy Irradionovich Casian is known to the general public as vice-chairman of Theoretical Physics Council at the Academy of Sciences of Moldova, vice-chairman of Specialized Council on PhD and Doctoral Theses in Theoretical Physics at the Academy of Sciences of Moldova, member of international editorial board of "Journal of Thermoelectricity" and other periodic scientific publications, head of the research group of four international projects.

In 1994 A.I. Casian was elected academician of the International Thermoelectric Academy, and in 1999 – a corresponding member of the American Romanian Academy of Arts and Sciences.

The well-known physicist was more than once invited for reading theoretical courses in the universities and institutes of France, Israel and USA.

The scope of the scientist's research interests is rather wide. They are related to fundamental problems of theory of semiconductors, transition phenomena and thermoelectric phenomena in low-dimensional structures, quantum wells, and thermoelectric properties of quasi-monomeric organic crystals.

The most significant innovative results have been achieved by the scientist in the following avenues of research:

– theory of kinetic and optical phenomena in polar semiconductors under dynamic screening conditions;

– thermoelectric effects in the structures with a large number of *p*-*n*-homo and heterojunctions;

– kinetics of current carriers and non-equilibrium carriers in ionizing radiation detectors;

– optical, transport and thermoelectric properties of some low-dimensional structures;

– thermoelectric properties of quasi-monomeric organic crystals.

Professor A.I. Casian is the author of over twenty scientific works, including two monographs and six textbooks.

The scientific, teaching and organizational activity of scientist A.I.Casian has been adequately assessed: he was awarded with a medal “For Valorous Labour” and many other state and public awards.

International Thermoelectric Academy, Institute of Thermoelectricity of the National Academy of Sciences and Ministry of Education and Science of Ukraine, “Journal of Thermoelectricity” Publishers cordially greet the esteemed Anatoliy Irradionovich on his glorious jubilee, sincerely wishing him sound health, happy longevity and new creative achievements.

## ARTICLE PREPARATION RULES

The article shall conform to the journal profile. The article content shall be legible, concise and have no repetitions.

The article shall be submitted to the editorial board in electronic version.

The text shall be typed in text editor not lower than MS Word 6.0/7.0.

Page setup: "mirror margins"- top margin – 2.5 cm, bottom margin – 2.0 cm, inside – 2.0 cm, outside– 3.0 cm, from the edge to page header – 1.27 cm, page footer – 1.27 cm.

Graphic materials, pictures shall be submitted in color or, as an exception, black and white, in .opj or .cdr formats, .jpg or .tif formats being also permissible. According to author's choice, the tables and partially the text can be also in color.

The article shall be submitted in English on A4 paper sheets; the number of pages shall not exceed 12. By agreement with the editorial board, the number of pages can be increased.

**To accelerate publication of the article, please adhere to the following rules:**

- the authors' initials and names are arranged in the centre of the first page at the distance of 1 cm from the page header, font Times New Roman, size 12 pt, line spacing 1.2;
- the name of organization, address (street, city, postal code, country) – indent 1 cm below the authors' initials and names, font Times New Roman, size 11 pt, line spacing 1.2, center alignment;
- the title of the article is arranged 1 cm below the name of organization, in capital letters, semi-bold, font New Roman, size 12 pt, line spacing 1.2, center alignment. The title of the article shall be concrete and possibly concise;
- the abstract is arranged 1 cm below the title of the article, font Times New Roman, size 10 pt, in italics, line spacing 1.2 ,center alignment;
- key words are arranged below the abstract, font Times New Roman, size 10 pt, line spacing 1.2, justified alignment. The title "Key words" – font Times New Roman, size 10 pt, semi-bold;
- the main text of the article is arranged 1 cm below the abstract, indent 1 cm, font Times New Roman. size 11 pt, line spacing 1.2, justified alignment;
- formulae are typed in formula editor, fonts Symbol, Times New Roman. Font size is "normal" – 12 pt, "large index" – 7 pt, "small index" – 5 pt, "large symbol" – 18 pt, "small symbol" – 12 pt). The formula is arranged in the text, centre aligned and shall not occupy more than 5/6 of the line width, formulae are numbered in round brackets right;
- dimensions of all quantities used in the article are represented in the International System of Units (SI) with the explication of the symbols employed;

• figures are arranged in the text. The figures and pictures shall be clear and contrast; the plot axes – parallel to sheet edges, thus eliminating possible displacement of angles in scaling;

• tables are arranged in the text. The width of the table shall be 1 cm less than the line width. Above the table its ordinary number is indicated, right alignment. Continuous table numbering throughout the text. The title of the table is arranged below its number, center alignment;

• references should appear at the end of the manuscript. References within the text should be enclosed in square brackets. References should be numbered in order of first appearance in the text. Examples of various reference types are given below.

– L.I. Anatychuk, *Thermoelements and Thermoelectric Devices: Handbook* (Kyiv: Naukova Dumka, 1979), p.766. (Book)
– T.M. Tritt, Thermoelectric Phenomena, Materials, and Applications, *Annual Review of Materials Research* **41**, 433 (2011). (Journal paper)
– U. Ghoshal, *Proceedings of the XXI International Conference on Thermoelectrics* (N.Y., USA, 2002), p. 540. (Proceedings Conference)

**The article should be supplemented by:**

• letter from the organization where the work was performed or from the authors of the work applying for the publication of the article;

• information on the author (authors): last name and initials; full name and postal address of the institution where the author works; academic degree; position; telephone number; E-mail;

• author's (authors') photo in color or, as an exception, in black and white. With the number of authors more than two their photos are not given;

• author's application to the following effect:

We, the undersigned authors, … transfer to the founders and editors of "Journal of Thermoelectricity" the right to publish the article…in Ukrainian, Russian and English. This is to confirm that the present publication does not violate the copyright of other persons or organizations.

Date Signatures